

ISVR Technical Memorandum

SCIENTIFIC PUBLICATIONS BY THE ISVR

Technical Reports are published to promote timely dissemination of research results by ISVR personnel. This medium permits more detailed presentation than is usually acceptable for scientific journals. Responsibility for both the content and any opinions expressed rests entirely with the author(s).

Technical Memoranda are produced to enable the early or preliminary release of information by ISVR personnel where such release is deemed to the appropriate. Information contained in these memoranda may be incomplete, or form part of a continuing programme; this should be borne in mind when using or quoting from these documents.

Contract Reports are produced to record the results of scientific work carried out for sponsors, under contract. The ISVR treats these reports as confidential to sponsors and does not make them available for general circulation. Individual sponsors may, however, authorize subsequent release of the material.

COPYRIGHT NOTICE

(c) ISVR University of Southampton All rights reserved.

ISVR authorises you to view and download the Materials at this Web site ("Site") only for your personal, non-commercial use. This authorization is not a transfer of title in the Materials and copies of the Materials and is subject to the following restrictions: 1) you must retain, on all copies of the Materials downloaded, all copyright and other proprietary notices contained in the Materials; 2) you may not modify the Materials in any way or reproduce or publicly display, perform, or distribute or otherwise use them for any public or commercial purpose; and 3) you must not transfer the Materials to any other person unless you give them notice of, and they agree to accept, the obligations arising under these terms and conditions of use. You agree to abide by all additional restrictions displayed on the Site as it may be updated from time to time. This Site, including all Materials, is protected by worldwide copyright laws and treaty provisions. You agree to comply with all copyright laws worldwide in your use of this Site and to prevent any unauthorised copying of the Materials.

UNIVERSITY OF SOUTHAMPTON INSTITUTE OF SOUND AND VIBRATION RESEARCH DYNAMICS GROUP

Wind tunnel tests on the noise radiated by cylinders with different cross-sections

by

E. Latorre Iglesias and D.J. Thompson

ISVR Technical Memorandum No. 1002

September 2014

Authorised issue by Prof. D.J. Thompson

© Institute of Sound and Vibration Research

Contents

1	Inti	roduction									
2	Exp	Experimental set-up									
	2.1	Repeatability									
	2.2	Background and shear layer noise correction									
	2.3	Effect of the changes in the effective cylinder length with the yaw angle \dots									
	2.4	Far-field and compact source assumption									
	2.5	Corrections for the directivity measurements									
3	Circ	cular cylinder									
	3.1	Noise spectra									
	3.2	Strouhal number									
	3.3	Amplitude of vortex shedding noise									
	3.4	Directivity of the vortex shedding noise									
4	Squ	Square cylinder									
	4.1	Noise spectra									
	4.2	Strouhal number									
	4.3	Amplitude of vortex shedding noise									
	4.4	Directivity of the vortex shedding noise									
	4.5	Angle of attack									
	4.6	Square cylinder with rounded edges									
5	Rec	Rectangular cylinders									
	5.1	Noise spectra									
	5.2	Strouhal number									
	5.3	Amplitude of the vortex shedding noise									
	5.4	Directivity of the vortex shedding noise									
6	Elli	ptical cylinders									
	6.1	Noise spectra									
	6.2	Strouhal number									
	6.3	Amplitude of vortex shedding noise									
	6.4	Directivity of the vortex shedding noise									
7	Bro	padband noise									
	7.1	Amplitude									
	7.2	Spectral shape									
	7.3	Directivity of broadband noise									
8	Sun	nmary of results									

Abstract

The phenomenon of vortex shedding from cylinders with different cross-sections has been extensively studied during the past years due to its application to many engineering fields. Many experimental works are reported in the literature and cover the aerodynamic parameters involved in the vortex shedding process from a cylinder such as Strouhal number, fluctuating forces and pressure distribution. The literature about the noise radiated by a cylinder undergoing vortex shedding is more scarce even though it has applicability to real cases such as the noise radiated by a high-speed train pantograph or an aircraft landing gear. The aim of the work presented is to extend the available experimental database on the noise radiated by cylinders with different cross-sections and different yaw angles inside an airflow, so they can be used for the validation of numerical prediction models and the validation and calibration of empirical and semi-empirical prediction models.

Wind tunnel tests were carried out in the ISVR anechoic wind tunnel on the noise radiated by circular, square, rectangular and elliptical cylinders when they are in an air flow undergoing a vortex shedding process. Flow speeds of 20, 25, 31.5, 40 and 50 m/s were used corresponding to Reynolds numbers in the range from 1.64×10^4 to 1.20×10^5 . The effect of the flow speed on the vortex shedding noise amplitude and frequency was assessed and the speed exponent α , which determines the rate of growth of the noise with the flow speed, was determined for each test case.

Unlike aircraft landing gear, in a train pantograph some of the struts are significantly inclined with respect to the incoming air flow. For this reason, the effect of the yaw angle on the noise radiated by all the cylinders has been assessed for angles of 30°, 45° and 60°, reaching angles of 75° in the case of the circular cylinder. The results obtained for the variation of the Strouhal number and noise amplitude at the vortex shedding frequency with the yaw angle have been compared to those given by the simplification proposed by the independence principle. Good agreement is found for the Strouhal number $(\cos(\beta))$ but there is some disagreement for the noise amplitude $(\cos^6(\beta))$.

For the case of the square cylinder the effect of the angle of attack on the noise radiation was assessed by rotating the cylinder about its axis by 10° , 15° , 30° and 45° . The vortex shedding was found to stop being triggered for an angle of attack between 10° and 15° . The effect of rounding the edges of the square cylinder was also assessed for angles of attack of 0° , 10° and 30° . It was found that the vortex shedding was always triggered, with an increase of the vortex shedding frequency and a decrease of the noise amplitude when the cylinder was rotated by 10° and the opposite trend for an attack angle of 30° .

The directivity of the noise radiated by each of the cylinders was measured for angles of radiation from 45° to 180°, in steps of 15°, where 90° is the position perpendicular to the flow direction. The results were compared with the directivity of a theoretical dipole source showing good agreement.

Not only the noise at the vortex shedding frequency but also the broadband noise was evaluated. The variation of the broadband noise radiated by each of the cylinders with the flow speed and yaw angle was assessed as well as the directivity of the broadband noise radiated by the circular and square cylinders. The speed exponent was also obtained and used in order to collapse the noise spectrum by the flow speed. By averaging the collapsed noise spectrum for each flow speed the spectral shape of the broadband noise for each of the cylinders and yaw angles was obtained so they can be used for the calibration and validation of semi-empirical prediction models.

List of symbols

C_L	rms fluctuating lift coefficient
C_0	rms coefficient of fluctuating lift for an right cylinder
c_0	Speed of sound (m/s)
d	Distance between the noise source and the observer (m)
D	Characteristic dimension of the cylinder (m)
e	Eccentricity of the elliptical cylinders
f_0	Vortex shedding frequency (Hz)
L	Effective length of the cylinder (m)
l_c	Spanwise correlation length of the surface pressure fluctuations (m)
l_{c_D}	Spanwise correlation length of the surface pressure fluctuations normalised by D
M	Mach number
$\overline{p^2(\underline{x})}$	Mean square sound pressure (Pa ²)
r	Radius of the rounded edges of the square cylinder (m)
Re	Reynolds number
S	Surface area (m^2)
SPL	Sound Pressure Level (dB, re 2×10^{-5} Pa)
St	Strouhal number
St_n	Normalised Strouhal number
U_{∞}	Mainstream flow speed (m/s)
$\underline{U_i}$	Mean flow speed measured at the i^{th} position (m/s)
$\underline{U_n}$	Component of the mainstream flow speed perpendicular to the cylinder (m/s)
$\underline{U_t}$	Component of the mainstream flow speed parallel to the cylinder (m/s)
\underline{x}	Position of the receiver with respect to the noise source (m)
α	Sped exponent

- β Yaw angle (°)
- λ Sound wavelength (m)
- ρ_0 Air density (kg/m³)
- ϑ Angle of attack (°)

1 Introduction

The aerodynamics of slender bodies such as cylinders with different cross-sections have been extensively studied in the past. Many experimental works have been reported on the fluctuating forces and Strouhal number related to the vortex shedding process undergone by cylinders with different cross-sections in an airflow. Experimental studies on the noise radiated by cylinders in such cases are less abundant even though they have an extensive application to real situations such as the aerodynamic noise produced by high-speed train pantographs or by aircraft landing gears. Databases based on noise wind tunnel tests, such as those presented by King et al. [1] and Hutcheson et al. [2], can be used for the validation of Computational Fluid Dynamics (CFD) and Computational AeroAcoustics (CAA) simulations or for the calibration and validation of semi-empirical and empirical prediction models. The aim of the work presented here is to extend the available experimental database on the noise radiated by cylinders with different cross-sections in an air flow. Results are presented for the effect of the cylinder yaw angle, the angle of attack or the inclusion of rounded edges in the case of a square cylinder, the dependence of the noise with the flow speed and the noise directivity.

Curle has shown that the noise generated by the fluctuating forces resulting from the interaction of an incident air flow with a solid body is equivalent with a distribution of dipole sources on the body's surface [3]. The sound intensity radiated by the dipole sources to the acoustic far-field can then be expressed in terms of $I \propto \rho_0 U_\infty^{\alpha} S d^{-2} c_0^{-3}$ where ρ_0 is the air density, U_∞ is the mean flow speed, α is the speed exponent, S is the surface area of the solid immersed in the air flow, d is the distance between the noise source and the receiver and c_0 is the speed of sound [3].

Different works have been carried out by Phillips [4], Etkin et al. [5] and Keefe [6] among others relating the fluctuating lift force and the noise radiated by a circular cylinder exposed to a cross-flow undergoing a vortex shedding process. The frequency of a sinusoidal fluctuating lift force can be expressed as $f_0 = StD/U_{\infty}$, where St is the Strouhal number of the vortex shedding process, D is the diameter of the circular cylinder and U_{∞} is the mean stream flow speed. The mean square sound pressure $(p^2(\underline{x}))$ radiated by a smooth circular cylinder in a cross-air stream at a certain position \underline{x} in the acoustic far-field can be expressed in terms of the rms fluctuating lift coefficient C_L , the spanwise correlation length of the surface pressure fluctuations l_c and the Strouhal number [4–6].

Following this approach, the following equation has been used to predict the noise radiated by a circular cylinder in an air flow at the vortex shedding frequency (peak noise level) by Fujita et al. [7] among others:

$$\overline{p^2(\underline{x})} = \frac{\rho_0^2 U_\infty^6 S t^2 C_L^2 L l_{c_D} D \sin^2(\theta)}{16c_0^2 d^2 (1 + M \cos(\theta))^4}$$
(1)

where ρ_0 is the air density, c_0 is the speed of sound, l_{c_D} is the spanwise correlation length of the surface pressure fluctuations as defined above but normalised by D. θ is the radiation angle defined as the angle between the flow direction and the line from the centre of the cylinder to the receiver, with $\theta = 0^{\circ}$ when the receiver is located in the flow direction upstream of the cylinder. The factor $\sin^2(\theta)$ represents the directivity of a theoretical dipole sound source that is used to represent the noise radiated by the fluctuating lift force and $(1 + M\cos(\theta))^4$ is the convective amplification factor for a moving dipole source.

Equation (1) is valid assuming a compact source, which in this case implies that the cylinder length should be much smaller than the acoustic wavelength λ of the radiated sound, and a far-field approximation, for which the distance between the cylinder and the observer d should be larger than the acoustic wavelength λ and the length of the cylinder [3]. Moreover, the cylinder is assumed to be rigid and not to vibrate so the normal surface velocity can be assumed to be zero and the Mach number M, defined as $M = U_{\infty}/c_0$, has to be small so the quadrupole noise sources representing the noise produced by the turbulent flow itself can be neglected [3].

The Reynolds number, defined as the ratio between the inertial forces and viscous forces in a flow, can be expressed as $Re = U_{\infty} \times D/\nu$, where ν is the kinematic viscosity of the fluid. The assumption of a purely sinusoidal fluctuating lift can be applied for Reynolds numbers within the subcritical region where the vortex shedding process is well localized around a specific frequency and the fluctuating lift spectrum has a tonal characteristic [8]. In the case of the critical and supercritical flow regimes the spectrum of the fluctuating lift broadens. Blake has proposed a method for the calculation of the noise spectrum radiated by the cylinder when the vortex shedding is irregular and the vortex shedding process is not localized at one specific frequency but over a broad frequency range [9].

The effects of the cylinder ends are not included in Eq. (1) where a cylinder with infinite length is considered or, at least, a cylinder with a sufficient aspect ratio L/D so the end effects can be neglected. The flow around the ends of the cylinder becomes three-dimensional and this affects the vortex shedding process along the cylinder leading to changes in the noise radiation. The effect of the cylinder aspect ratio on the noise radiated by cylinders of different cross-sections was studied empirically by King and Pfizenmaier [1].

The effect of the cylinder yaw angle on the noise radiation is of special interest. The yaw angle (β) is here defined as the angle between the line perpendicular to the flow direction and the cylinder axis, i.e. a yaw angle of 0° means that the cylinder is perpendicular to the flow. Following the examples given above, the struts that are part of, for example, an aircraft landing gear or, to a greater extent, a high-speed train pantograph are inclined with respect to the incoming flow. An approximation to assess the effect of the yaw angle on the Strouhal number and the amplitude of the vortex shedding noise that is used for engineering purposes is known as the *independence principle*. It is assumed that, for flow over a cylinder with a certain yaw angle, the vector of the mean stream incident flow speed \underline{U}_{∞} can be decomposed into two perpendicular components, \underline{U}_n that is perpendicular to the yawed cylinder centreline and \underline{U}_t that is parallel to it [8]. The normal flow speed component can be expressed in terms of the mean stream flow speed and the yaw angle:

$$U_n = U\cos(\beta) \tag{2}$$

Substituting the expression above in Eq. (1) yields the dependency of the amplitude of the mean square sound pressure on the yaw angle which can be expressed simplistically as $\overline{p^2(\underline{x})} \propto U^6 \times \cos^6(\beta)$. However, the variation of the incident flow speed will lead to changes in the Reynolds number that may modify the rms fluctuating lift coefficient and the correlation length, leading to additional changes in the noise amplitude.

In order to make the Strouhal number independent of the yaw angle, in subsequent analysis the term normalised Strouhal number will be used as defined by:

$$St_n = St \times \cos \beta \tag{3}$$

According to that, for a certain yaw angle β , then the normalised Strouhal number should be exactly the same as St for a cylinder perpendicular to the flow.

In this report results are presented of tests carried out in the Institute of Sound and Vibration Research (ISVR) anechoic wind tunnel on the noise radiated by cylinders with different cross-sections: circular, square, rectangular and elliptical cylinders for five different flow speeds: 20, 25, 31.5, 40 and 50 m/s, corresponding to a Reynolds number range from 1.64×10^4 to 1.20×10^5 . This allowed an assessment of the dependence of the noise radiated by the different cylinders on the flow speed and the Reynolds number in the range covered during the experiments.

The effect of inclining the cylinder with respect to the incident flow is evaluated for yaw angles of 0° , 30° , 45° , 60° and 75° . The results obtained for the variation of St and the Sound Pressure Level (SPL) with the yaw angle are compared with those expected from the application of the independence principle in order to assess the suitability and accuracy of this simplification. The effect of the angle of attack is assessed for a square cylinder with sharp edges and edges rounded using a radius of D/12. The directivity of the vortex shedding noise radiated by the cylinders is also assessed and the results are compared with the directivity of a theoretical dipole source.

The analysis involves not only the noise at the vortex shedding frequency but also the broadband noise generated by the vortex shedding process. The variation of the broadband noise with the flow speed and yaw angle is assessed, together with the directivity of the broadband noise radiated by the circular and the square cylinders.

The database obtained here is intended mainly to be used for the calibration of semi-empirical models for the prediction of the aerodynamic noise radiated by components of the pantograph of a high-speed train. In that sense, the noise produced by the fluctuating drag was not accounted for as its radiation axis lies in the flow direction, so its impact on the wayside noise produced by a passing-by train can be neglected. Other factors that can affect the noise radiation from the cylinder such as roughness, vibration and free-stream turbulence have not been evaluated.

Section 2 describes the experimental set-up. Results at the vortex shedding frequencies are presented for different cross-sections in Section 3-6. Broadband noise is discussed in Section 7.

2 Experimental set-up

The experiments were carried out in the ISVR open jet anechoic wind tunnel. This facility provides a high speed flow with low background noise and low turbulence level [10]. The size of the rectangular nozzle was 0.35 by 0.50 m, which has limited the effective length of cylinder (L) defined as the length of the segment of the cylinder placed inside the clean flow - and characteristic dimension (D) - defined as the dimension of the cylinder transverse to the flow direction - that could be used. For all the cases under test different flow speeds were used (20, 25, 31.5, 40 and 50 m/s) in order to assess the speed dependence of the noise radiated by the cylinders and to cover a broader Reynolds number range.

Figure 1 shows the cross-section of the different cylinders used during the tests and their characteristic dimensions. The identifier for each of the cases is shown at the bottom left corner: C stands for the circular cylinder, S for the square cylinder, Sr for the square cylinder with rounded edges with radius (r) of D/12, R1 and R2 for the rectangular cylinders with aspect ratios of 1.33 and 2.0 and E1 and E2 for the elliptical cylinders with eccentricities of 0.63 and 0.75 (the eccentricity is defined as $e = \sqrt{1 - b^2/a^2}$). The circular and square cylinders were made of steel and the rectangular and elliptical cylinders were made of wood, all the cylinders having a smooth surface.

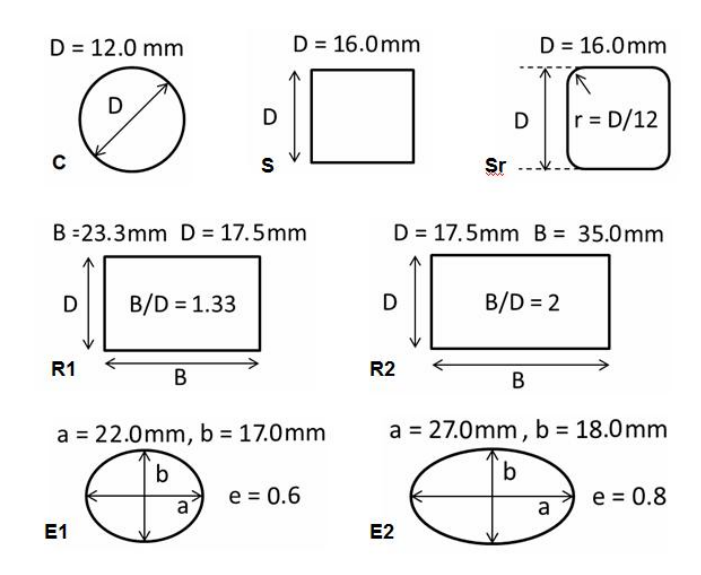


Figure 1: Cross-section, characteristic dimension (D) and identifier of the cylinders used during the wind tunnel tests.

Figure 2 a) and Figure 2 b) show the definition of the angle of attack (ϑ) and the yaw angle (β) as used in this report. Yaw angles of 15°, 30° and 45° and 60° were used for all the cylinder configurations and an additional angle of 75° was evaluated in the case of the circular cylinder. The yaw angle is included in the identifier of the different test cases by adding Y followed by the value of the angle, i.e. C+Y45 stands for a circular cylinder with a yaw angle of 45°. Angles of attack of 10°, 15°, 30° and 45° were measured for the square cylinder with sharp edges and angles of attack of 10° and 30° for the square cylinder with rounded edges. In the case of rectangular cylinders an angle of attack of 90° was used in order to obtain a right rectangular cylinder with a different aspect ratio (0.5 and 0.75). In this case the identifier was modified by adding A followed by the angle of attack. For example, S+A15 stands for the square cylinder with an angle of attack of 15°. Symmetry was assumed in terms of rotating the square cylinder in the upstream (negative angles of attack) or downstream (positive angles of attack) direction.

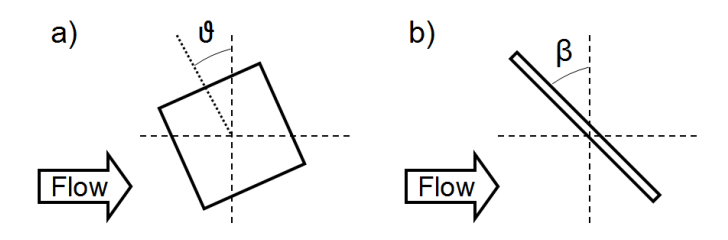


Figure 2: Sketch showing the definition of: a) The angle of attack ϑ . b) The yaw angle β .

Figure 3 shows the experimental set-up used. The cylinders were attached to two vertical stands, as shown in Figure 3 a), that were placed outside the flow to avoid unwanted noise from the

interaction between the air flow and the stands. Both stands were wrapped with sound absorptive foam to minimize the effect of any reflection of the noise coming from the cylinder. The floor beneath the cylinder was covered with wedges of sound absorptive material for the same reason. An array of eight microphones was placed lengthwise with respect to the air flow direction and a second array of four microphones was positioned transversally to the flow direction, as shown in Figure 3 b). Microphone 4 was used for all the analysis included in this report as its position is perpendicular to the flow from the cylinder position so the effects of the convective amplification and the shear layer refraction can be neglected. The rest of the microphones included in the array were used for the directivity measurements.

No end plates were used on the cylinders, in order to increase the angles covered in the directivity measurements. However this makes it important to assess the effect of the jet shear layer impinging on the cylinder. Not only may this lead to an increment in the noise produced but it may also affect the assumption that the aspect ratio is high enough to allow neglect of the end effects so that the cylinder can be approximated as infinitely long.



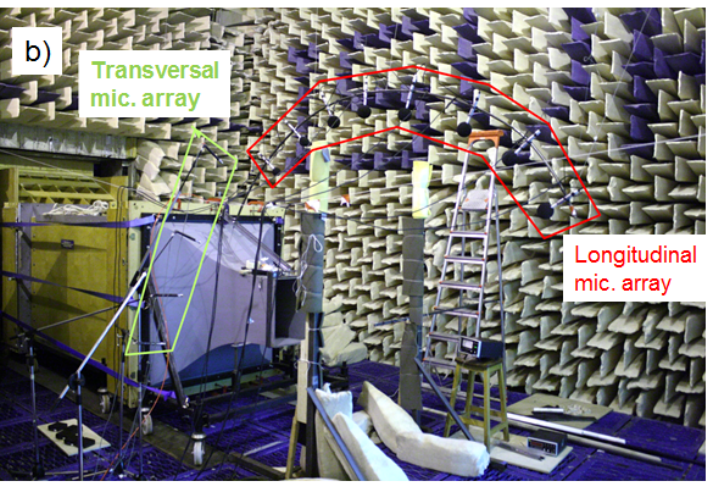


Figure 3: a) Rear view of the experimental set-up showing the stands holding the cylinder for the configuration S+Y60 and the absorptive foam wedges placed on the ground to minimize the sound reflections from the floor grids. b) General view of the experimental set-up showing the longitudinal and the transversal microphone arrays used for the directivity measurements.

The sketches shown in Figure 4 detail the position of each of the microphones with respect to cylinder. For the directivity measurements angles between 45° and 150° were covered in the flow stream direction in steps of 15°. In order to cover higher angles the transversal array was used because, if the longitudinal array is used for higher angles than 150°, then the microphones will be placed inside the air flow (leading to an increase of the background noise due to the wind noise). Angles lower than 45° were not used as the nozzle would scatter and screen the sound from the cylinder. The transversal array covered angles from 135° to 180° in steps of 15° and, in order to avoid the screening effect of the stands, the microphones were placed 7° upstream of the cylinder. Symmetry in both the parallel and the transverse directions was assumed for the directivity of the noise radiated by the cylinder. Both arrays covered the angles of 135° and 150° so, by comparing the results obtained, this symmetry can be verified.

The microphones were connected to a microphone preamplifier providing the necessary power

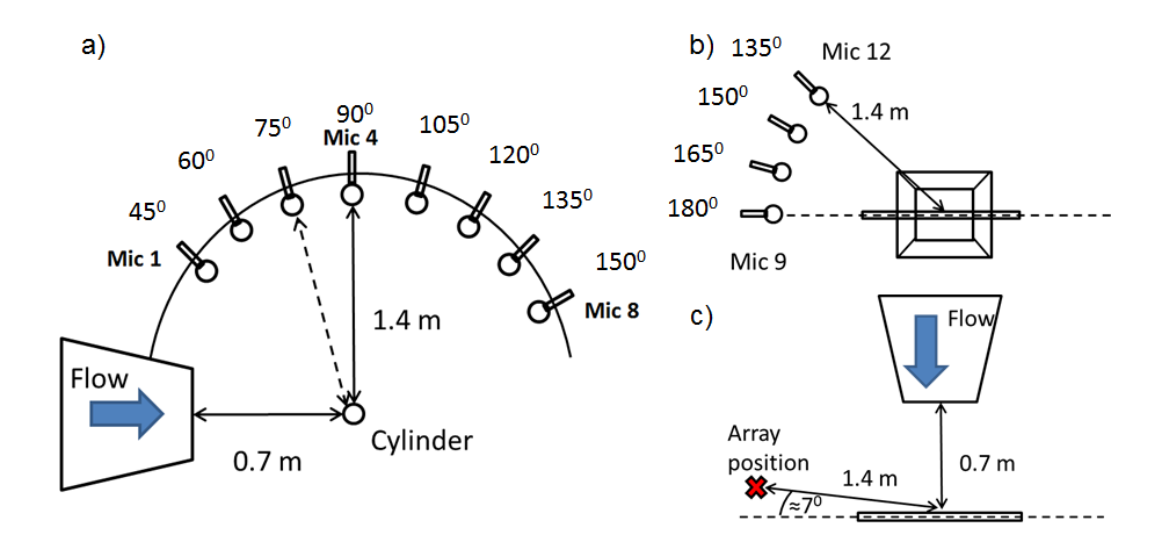


Figure 4: Sketches of the experimental set-up. a) Sketch of the side view showing the relative position of each of the microphones of the longitudinal array with respect to the cylinder. b) Sketch of the front view showing the microphones of the transversal array with respect to the cylinder. c) The microphones of the transversal array were located 7° upstream of the cylinder to avoid screening of the sound by the stands.

supply. The output of the amplifiers was connected to a multichannel acquisition system, which was controlled using a PC. The whole measurement chain was calibrated for each of the input channels using a microphone calibrator emitting a pure tone of 94 dB at 1 kHz. Time signals of 10 seconds duration for each of the input channels were acquired using a sample frequency of 48 kHz. The noise power spectral density (PSD) was calculated using Welch's method, a Hanning window of 8,192 samples and a block overlap of 50%, to give a frequency resolution of 5.86 Hz. Then the results were converted to noise spectra by multiplying the PSD by the frequency resolution and subsequently converted to 1/3 octave bands by summing up the amplitude of each of the frequency lines inside each 1/3 octave band.

All the results shown in this report, unless otherwise stated, correspond to the maximum value of the noise spectrum, which is the noise level of the vortex shedding peak. For the results related with the Strouhal number the vortex shedding frequency was chosen as the frequency where the narrow band spectrum was maximum. Nevertheless, for the amplitude analysis the maximum amplitude of the 1/3 octave band noise spectrum was chosen.

Table 1 shows the Reynolds number range covered during the experiments for the different cylinder cross-sections. The characteristic dimension (D) used for each of the cylinders is also listed. In the case of the circular cylinder it must be pointed out that all the measurements were made in the subcritical region. It would be interesting to extend the Reynolds number range to the critical range or to the transition between the critical and subcritical range but it was not possible due to the limitations in the maximum flow speed and the actual aspect ratio that could be used (due to the nozzle size).

Table 1: Reynolds number for the different cylinder cross-sections and flow speeds used. The

1	1	\boldsymbol{T}		1		
characteristic	dimension	1)	18	expressed	ın	mm.

	Cylinder		Flow speeds (m/s)					
Cross-section	Identifier	D (mm)	20	25	31.5	40	50	
Circular	С	12.0	1.64×10^4	2.05×10^4	2.59×10^4	3.29×10^4	4.11×10^4	
Square	S & Sr	16.0	2.19×10^4	2.74×10^4	3.45×10^4	4.38×10^4	5.48×10^4	
Rectangular	R1 & R2	17.5	2.40×10^4	3.00×10^4	3.78×10^4	4.79×10^4	5.99×10^4	
Rectangular	R1+A90	23.3	3.19×10^4	3.99×10^4	5.03×10^4	6.37×10^4	7.97×10^4	
Rectangular	R2+A90	35.0	4.80×10^4	6.00×10^4	7.56×10^4	9.58×10^4	1.20×10^5	
Elliptical	E1	17.0	2.33×10^4	2.91×10^4	3.67×10^4	4.66×10^4	5.82×10^4	
Elliptical	E2	18.0	2.47×10^4	3.08×10^4	3.88×10^4	4.93×10^4	6.16×10^4	

2.1 Repeatability

Figure 5 shows the comparison between measurements carried out on two different days using the right circular cylinder and the right rectangular cylinder with an aspect ratio of 1.33 for different flow speeds. The results shows a good repeatability.

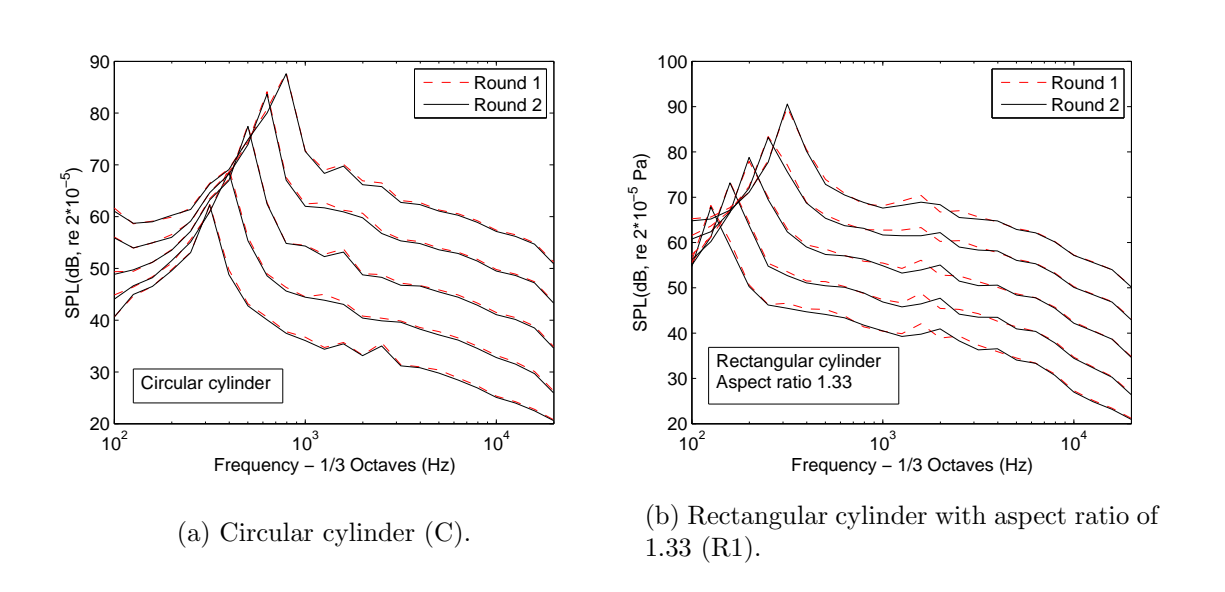


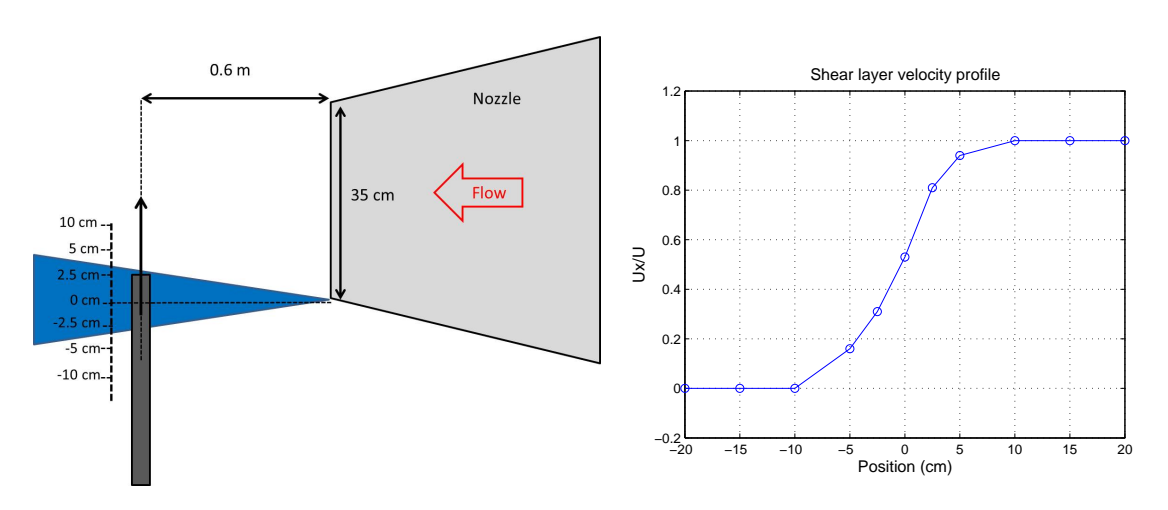
Figure 5: 1/3 octave band noise spectra radiated by the right circular cylinder and the right rectangular cylinder with aspect ratio of 1.33 for different flow speeds, showing the repeatability of the results. Results shown for five different flow speeds.

2.2Background and shear layer noise correction

The background noise was considered as the noise when all the elements of the experimental set-up were included except for the cylinder itself. It was measured for all the flow speeds used during the tests. Because the position of the stands changed depending on the yaw angle to be tested, the background noise was measured independently for each of these configurations.

End plates were not used in order to be able to measure the directivity of the noise in the transversal plane, as shown in Figure 4 b) and Figure 4 c). The absence of end plates means that

a turbulent mixing shear layer exists at both sides of the air stream. Since the cylinders used were longer than the nozzle width, the interaction between the turbulent shear layer and the cylinder is susceptible to produce broadband noise. Even though this will not be significant compared to the vortex shedding peak noise, it may contribute to the broadband noise measured. If the broadband noise from the cylinder is to be measured then it is important to assess the contribution of the shear layer interaction noise. To do that, the flow velocity profile at positions inside the shear layer was measured using a Pitot tube. Different crosswise positions were covered through the shear layer at a distance of 0.6 m from the nozzle edge, as shown in Figure 6 a). The flow speed profile obtained is shown in Figure 6 b).



- (a) Position where the flow speed was measured cross wise the shear layer.
- (b) Shear layer velocity profile. U_i is the mean flow speed measured at the ith position and U_{∞} is the main stream flow speed.

Figure 6: Set-up used for the shear layer velocity profile measurements and results obtained.

It was assumed that the end of the shear layer roughly corresponds to the position 3.5 cm where the measured flow speed was approximately 90% of the mainstream flow speed. Next, the noise was measured when the end of the cylinder was inserted into the flow with the tip of the cylinder placed at the position 3.5 cm (hereafter called shear layer noise) and it was used for the shear layer noise correction. Figure 7 shows the background noise and shear layer noise measured for the right circular cylinder for two different flows speeds: 31.5 and 50 m/s. Only the shear noise of one of the cylinder ends was measured and it was assumed that the other end of the cylinder will produce an identical shear layer interaction noise, so the overall shear layer noise was estimated as 3 dB higher than the measured spectrum.

The shear layer noise measured was also corrected to allow for the background noise. Then the background noise was incoherently summed to twice the measured shear layer noise, and the result was used to correct the noise measured when the right circular cylinder was installed in the air flow. It can be seen that the correction does not affect the vortex shedding peak. Its effect is strong for frequencies below the vortex shedding peak and it affects some of the frequency bands above the vortex shedding peak. For some cases at lower speeds, in some specific frequency bands, the subtraction of the background noise from the noise from the cylinder is not possible reliably because the difference between them is less than 3 dB. To simplify matters, due to the fact that the quantity of data to analyze is large, no correction was applied for any frequency and the broadband noise is only considered for frequencies higher than the shedding frequency, as for lower frequencies the signal to noise ratio achieved is not high enough. It can be concluded that

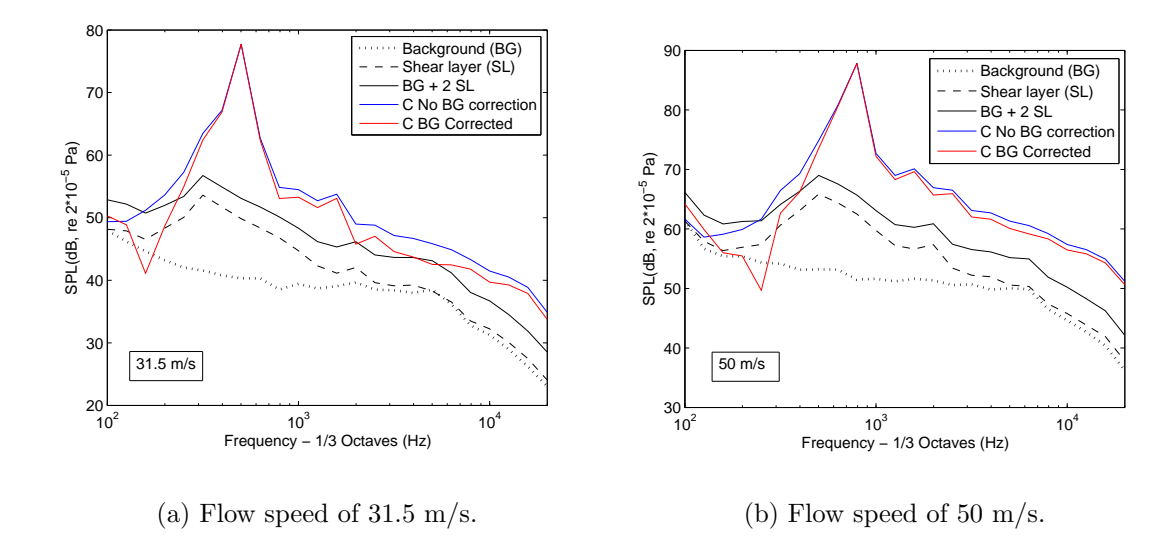


Figure 7: Noise spectrum measured for the right circular cylinder. The background noise and shear layer noise is detailed and the effect of the background noise and shear layer noise correction on the noise radiated by the cylinder is shown.

the background noise (including the shear layer noise) is negligible at the vortex shedding peak noise and it is not significant in most of the cases for the broadband noise for frequencies above the vortex shedding frequency.

The shear layer was assumed to have a thickness with constant growth downstream of the nozzle so the surface of the cylinder inside the shear layer (taking into account both ends of the cylinder) remained constant when the cylinder was yawed with respect to the flow direction.

The interaction between the jet shear layer and the cylinder could produce end effects leading to the reduction of the effective aspect ratio that can be considered. This effect was not taken into account in the present work.

2.3 Effect of the changes in the effective cylinder length with the yaw angle

Although the characteristic dimension of all the cylinders was kept constant during the tests, the effective length of the cylinder has increased with the increase of the yaw angle. Table 2 shows the length (L) and aspect ratio (L/D) for each of the yaw angles and for each of the cylinders used.

As was shown in Eq. (1), the noise radiated by the cylinder is proportional to its length (L). A correction factor of

$$SPL_{lengthcorrection} = 10 \log_{10}(L_r/L_{ti}) \simeq 10 \log_{10} \cos \beta$$
 (4)

was applied to compensate for the increase in the effective length of the cylinder inside the clean flow with the increase of the yaw angle, where L_r is the effective length of the right cylinder and L_{ti}

Table 2: Length and aspect ratio for each of the yaw angles and for each of the cylinders used during the experiments.

	Yaw angle (β)				
	0°	30°	45°	60°	75°
Effective length L (cm)	26.4	31.8	40.9	61.4	126.6
L/D C	22.0	26.5	34.1	51.2	105.5
m L/D~S~and~Sr	16.5	19.9	25.6	38.4	_
m L/D~R1	15.1	18.2	23.4	35.1	_
m L/D~R2	15.1	18.2	23.4	35.1	_ _
m L/D~E1	15.6	18.7	24.1	36.1	_
m L/D~E2	14.7	17.7	22.7	34.1	_

is the effective length of the cylinder yawed by i degrees. This correction factor was only applied to the overall SPL when the results were compared between different yaw angles but it was not applied to the narrow band or 1/3 octave band noise spectra. The fluctuating lift coefficient and the correlation length are assumed to be independent of the cylinder length for sufficiently high cylinder aspect ratios so the end effects can be neglected. The length of the cylinder included in Table 2 is the result of subtracting the width of the shear layer from the length of the cylinder inside the area delimited by the nozzle width. In the present tests the effect that the interaction between the jet shear layer and the cylinder can have in terms of introducing end effects and reducing the effective aspect ratio L/D were not accounted for.

Table 3 shows the effective length of the cylinder for the different yaw angles and the correction applied (Eq. (4)).

Table 3: Amplitude correction (expressed in dB) to account for the increment of the length of the cylinder inside the flow when the yaw angle increases.

	Yaw angle (β)							
	0°	30°	45°	60°	75°			
Length L (cm)	26.4	31.8	40.9	61.4	126.6			
Correction (dB)	0.0	-0.6	-1.5	-3.0	-5.9			

2.4 Far-field and compact source assumption

If microphone number 4 is considered, which is used for all the analysis included in this report, the distance between the microphone and the centre of the cylinder is 1.4 m. When the cylinder is yawed this distance remains constant and the distance to the ends increases. For most of the configurations the distance between microphone 4 and the centre of the cylinder is at least twice the effective length of the cylinder (shown in Table 2 and Table 3) so the the geometrical far-field condition is satisfied. However, for a yaw angle of 75° this condition may not be satisfied as the effective length of the cylinder is close to the distance between microphone 4 and the centre of the cylinder.

Table 4 shows the maximum and minimum vortex shedding frequency (f_0) and wavelength (λ) obtained for each of the cylinders, which correspond to the vortex shedding frequency obtained for the maximum and minimum flow speeds, i.e. 50 and 20 m/s.

Table 4: Maximum and minimum vortex shedding frequency (f_0) and corresponding wavelength (λ) found for the different cylinders under test.

	Max. $f_0(Hz)$	Min. $f_0(Hz)$	Min. $\lambda(m)$	Max. $\lambda(m)$
$^{-}$ CC	755	105	0.45	3.24
SC	386	76	0.88	4.47
EC e = 0.63	539	111	0.63	3.05
EC e = 0.75	978	111	0.35	3.00
RC AR= 1.33	310	82	1.09	4.15
RC AR= 0.75	216	58	1.57	5.80

Looking at the results shown in Table 4 a range of acoustic wavelengths from 5.8 m to 0.4 m is covered. This shows that for the lowest flow speeds and yaw angles for the square, rectangular and elliptical cylinders, the conditions of the acoustic far field, that is, $d>>\lambda$, are not strictly satisfied.

Comparing the effective length of the cylinder shown in Table 2 and the acoustic wavelengths of the vortex shedding noise shown in Table 4, for most of the cases the cylinder can be considered as an acoustically compact source as $L \ll \lambda$. This condition may not be satisfied for the case of the circular cylinder at the yaw angle of 75°.

In the case of the directivity measurements, which have been carried out using all the microphones included in the set-up, these conditions are not satisfied for some of the microphones, especially those of the transversal microphone array. This has to be considered when analysing the results obtained.

2.5 Corrections for the directivity measurements

The data have been corrected to eliminate the effects of the jet shear layer refraction and the convective amplification. For the shear layer refraction correction, the method developed by Amiet [11] was applied assuming a plane zero-thickness shear layer. The convective amplification was corrected using the theoretical factor $(1 + M \cos \theta)^{-4}$ for the squared sound pressure radiated by a moving dipole (see Eq. (1)).

Tables 5 and 6 show the corrections applied for each of the microphones of the longitudinal array (microphones 1 to 8). For the transversal array a negligible influence of both shear layer and convective amplification was assumed.

Table 5: Shear layer refraction correction, dB.

	Flow speed (m/s)						
Mic. number	θ	20	25	31.5	40	50	
1	45°	1.1	1.3	1.7	2.1	2.6	
2	60°	0.7	0.9	1.1	1.4	1.7	
3	75°	0.4	0.4	0.5	0.7	0.9	
4	90°	0.0	0.0	0.0	0.0	0.0	
5	105°	-0.3	-0.4	-0.5	-0.6	-0.8	
6	120°	-0.7	-0.8	-1.1	-1.4	-1.7	
7	135°	-1.1	-1.4	-1.7	-2.2	-2.8	
8	150°	-1.8	-2.3	-2.7	-3.1	-3.5	

Table 6: Convective amplification correction, dB.

	Flow speed (m/s)						
Mic. number	θ	20	25	31.5	40	50	
1	45°	-0.7	-0.8	-1.1	-1.4	-1.8	
2	60°	-0.5	-0.6	-0.8	-1.0	-1.3	
3	75°	-0.3	-0.3	-0.4	-0.5	-0.7	
4	90°	0.0	0.0	0.0	0.0	0.0	
5	105°	0.3	0.3	0.4	0.5	0.7	
6	120°	0.5	0.6	0.8	1.1	1.4	
7	135°	0.8	0.9	1.1	1.5	1.9	
8	150°	0.9	1.1	1.4	1.9	2.4	

Microphones 7 and 8 can be compared directly with microphones 12 and 11 that are located in a different plane but at the same radiation angle (θ) with respect to the cylinder. In this case, symmetry in the directivity pattern is supposed.

3 Circular cylinder

3.1 Noise spectra

Figure 8 shows the narrow band noise spectra radiated by the circular cylinder for different yaw angles and different flow speeds. These data were not corrected for background noise and shear layer noise. As expected, as the yaw angle increases the vortex shedding frequency decreases and the vortex shedding peak broadens. It can been seen how the broadband noise at frequencies above the vortex shedding frequency also decreases with the increasing yaw angle, except for the yaw angle of 75° for which the broadband noise is dominated by the background noise. Hogan and Hall [12] found that the broadband noise component of the fluctuating wall pressure along the cylinder increased with the yaw angle at frequencies below the vortex shedding frequency. However the noise radiated by the cylinder at frequencies below the vortex shedding frequency could not be assessed in the present work due to the low signal to noise ratio.

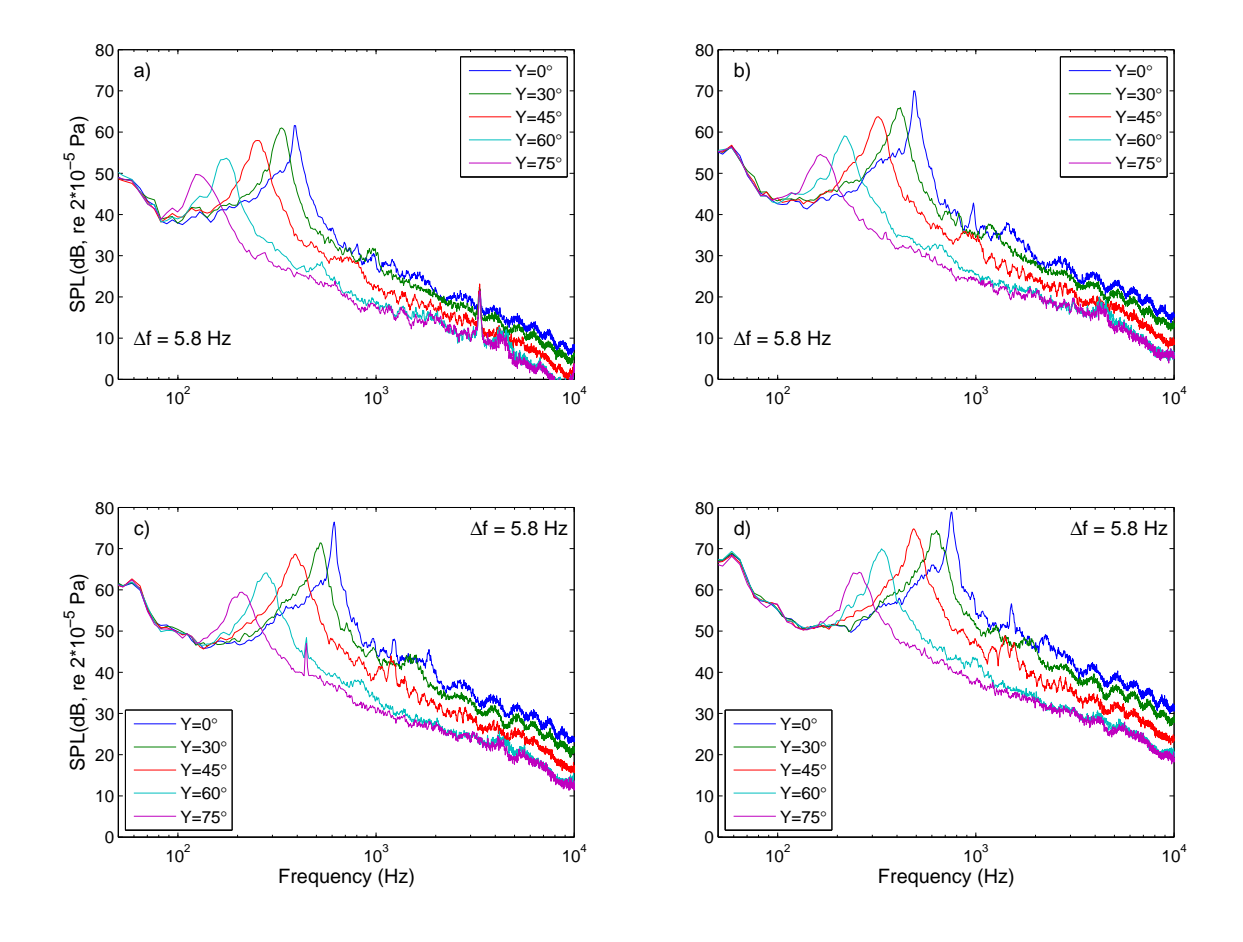


Figure 8: Narrow band noise spectra radiated by the circular cylinder for different yaw angles and flow speeds. (a) 25 m/s. (b) 31.5 m/s. (c) 40 m/s. (d) 50 m/s.

3.2 Strouhal number

The vortex shedding frequency has been extracted from the narrow band noise spectra and expressed as a normalised Strouhal number based on the cylinder diameter. The normalised Strouhal number was calculated according to the Eq. (3). The variation of the Strouhal number with the Reynolds number is shown in Figure 9 a). The frequency resolution of 5.8 Hz means that St is determined to within at least 2 or 3%.

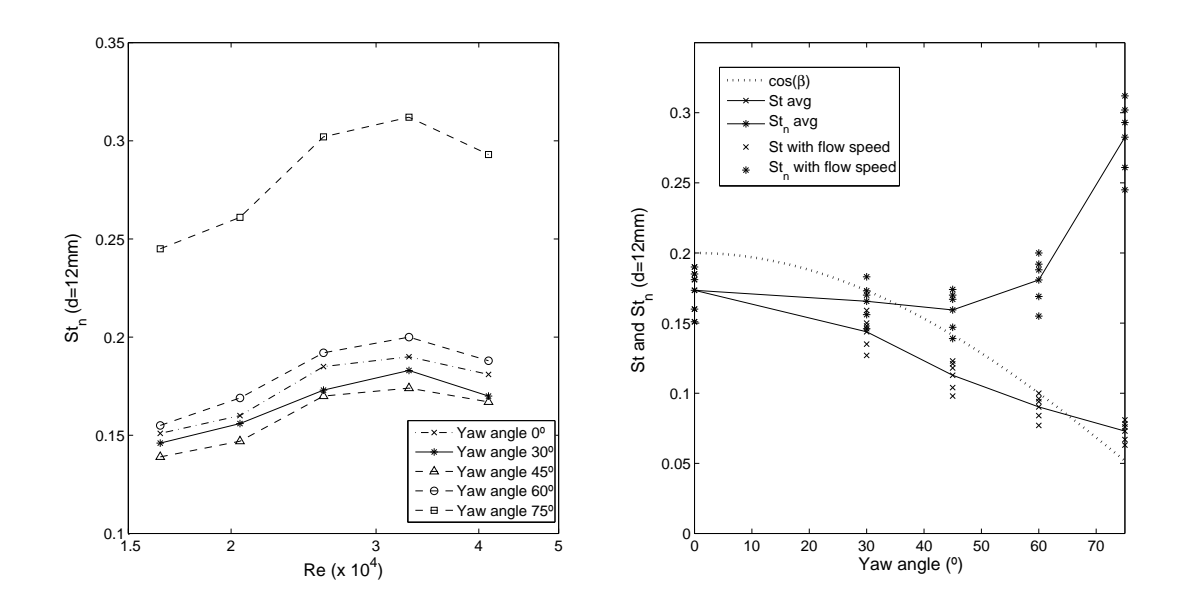


Figure 9: Variation of the St_n and St with the flow speed and yaw angle for the circular cylinder. a) St_n versus flow speed. b) Variation of the St and St_n with the yaw angle compared to those expected using the theoretical factor $\cos(\beta)$.

The Strouhal number, even if it undergoes a slight increase for the highest Reynolds numbers, is lower than the value of 0.2 obtained by Schewe [13], among others, from the measurement of the rms fluctuating lift coefficient in the same Reynolds number range. This disagreement could be due to the fact that the aspect ratio (L/D) used in the current experiments is not high enough to allow the end effects to be neglected. Gowda found that the three-dimensional flow produced by the cylinder free ends affected the Strouhal number of the vortex shedding produced by a circular cylinder in an air flow [14]. Gowda found that an aspect ratio L/D above 45 is necessary to obtain the same Strouhal number as those measured using end-plates. However, King and Pfizenmaier found that, with an aspect ratio L/D of 25, the Strouhal number obtained from the vortex shedding noise produced by a circular cylinder with a single free end in an air flow was the same as those measured with end plates [1]. However, in the present work, the fact that the normalised Strouhal number is also lower when the cylinder is yawed, even though the aspect ratio increases substantially, does not clarify the reason for this disagreement.

It should be highlighted that the normalised measured Strouhal number is significantly higher for a yaw angle of 75°. This increase of the Strouhal number could be a consequence of changes in the flow behaviour around the cylinder but this was not proven. The vibration of the cylinder could also affect the Strouhal number obtained but this was not measured. In the case of the yaw angle of 75°, the vibration of the cylinder could be more significant than for lower yaw angles because the cylinder used was quite long (around 3 m long between supports, with an effective length of around 1.3 m) and quite flexible. The fluctuating lift can be affected by the cylinder vibration depending

on the amplitude of the displacement of the cylinder, the relationship between the vortex shedding frequency and the natural frequencies of the cylinder and the Reynolds number [9]. Blake shown that, when the vortex shedding frequency is close to the resonance frequency of the cylinder, small variations of the flow speed may not vary the frequency of the noise spectrum peak as it is close to the natural frequency of the cylinder [9]. Increasing the flow speed sufficiently the noise spectrum peak due to the vortex shedding frequency will again be distinguishable. However, the fact that the noise spectrum peak frequency changes with the flow speed and high Strouhal numbers are found for all these flow speeds seems to show that the noise spectrum peaks are independent of the natural frequencies of the cylinder.

Figure 9 b) shows the variation of the average Strouhal number (averaged over the five flow speeds tested) with the yaw angle in comparison with the theoretical factor $\cos \beta$ defined by the independence principle. The Strouhal number normalised by this factor, St_n , is also shown. There is a significant variability of the results with the flow speed, with variations of around 20% in some cases. The comparisons with the factor $\cos \beta$ shows a reasonable agreement in the trend followed for angles lower than 45°, with a significant disagreement for the angles of 60° and especially 75°.

3.3 Amplitude of vortex shedding noise

Figure 10 shows the variations of the SPL in the 1/3 octave band of the vortex shedding peak with the flow speed. The speed exponent (α) , calculated from the slope of the straight line obtained after applying linear curve fitting, is listed in Table 7 for each of the yaw angles.

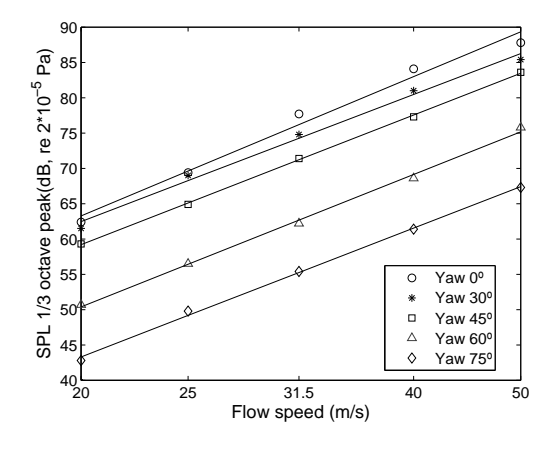


Figure 10: Changes in the SPL with the flow speed for the circular cylinder.

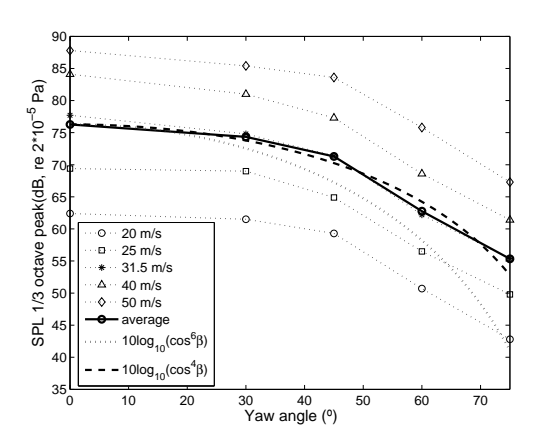
Table 7: Speed exponents for the different yaw angles for the circular cylinder.

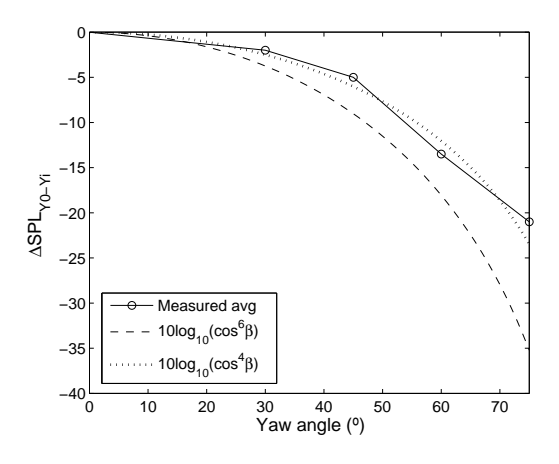
CIRCULAR CYLINDER								
Speed exponent (α)								
6.5								
6.0								
6.1								
6.2								
6.1								

The speed exponents obtained are quite close to the value of 6 for a theoretical dipole source, as expected for the noise generated by a fluctuating force, except for the yaw angle of 0° . In this

case, a value of 6.5 is obtained. However in this case it can be seen in Figure 10 that the speed dependence does not correspond to a simple linear trend. The reason for this is unknown.

Figure 11 a) shows how the SPL of the vortex shedding peak decreases when the yaw angle increases. It can be seen that the trend followed is similar for all the flow speeds. However, if these results are compared with the theoretical value expected from the independence principle, as shown in Figure 11 b), the results strongly disagree. Figure 11 b) shows the trend of the difference between the SPL radiated by the circular cylinder yawed by different angles and the right circular cylinder ($\Delta \text{ SPL}_{\beta_i-\beta_0}$ where β_i is the ith angle of attack and β_0 is the angle of attack of 0°). The results have been averaged for the different flow speeds and they are compared with different powers of the factor $\cos \beta$. It seems that the exponent that better matches the average experimental results is 4 instead of 6.





- (a) SPL versus yaw angle for different flows speed.
- (b) Comparison between the variation of the average SPL with β and different powers of the factor $\cos(\beta)$.

Figure 11: Variation of the SPL of the vortex shedding noise with the yaw angle. The effect of the different effective length of the cylinder for the different yaw angles was previously corrected using the correction factor shown in Eq. (4).

Another point to be mentioned is the relatively high SPL obtained for the yaw angle of 75° compared with that expected if the SPL is to be decreased by the factor $\cos^{6}\beta$ or even by the factor $\cos^{4}\beta$. In this case, the length of the cylinder (around 3 m) and the small diameter (12 mm) made it quite flexible and prone to vibrate. The effect of the vibration of the cylinder can increase the amplitude of the fluctuating lift coefficient and the correlation length for sufficiently high amplitudes of vibration [15]. In this case the vibration undergone by the cylinder was not measured so it cannot be stated whether this increase with respect to the expected SPL for a yaw angle of 75° is due to changes in the flow behaviour or due to the effect of the vibration of the cylinder. Additionally when the cylinder is yawed by 75° the compact source approximation is not fulfilled. This may affect to the amplitude of the measured noise. However, in this situation the noise radiated would be lower than if the compact source approximation is satisfied so this does not explain the high noise level obtained for a yaw angle of 75° .

3.4 Directivity of the vortex shedding noise

Figure 12 shows the directivity measured for the right circular cylinder in the 1/3 octave band where the vortex shedding peak was located. The directivity for all the flow speeds is included. The results are shown as the difference in the SPL between an angle θ_i , the i^{th} angle of radiation, and θ_0 the angle of radiation of 90°. These results are compared with the directivity expected for a theoretical dipole source. Good agreement is found in the comparison even though for some of the angles the dispersion in the results is around +/- 3 dB. A good agreement is found if the results from the two different microphone arrays are compared (for 135° and 150°) confirming the symmetry in the noise radiation between the longitudinal and the transversal plane with respect to the flow direction. It must be noticed that no noise is expected at 180° according to the theoretical dipole directivity pattern but, in the case of the measured data, the background noise is contributing.

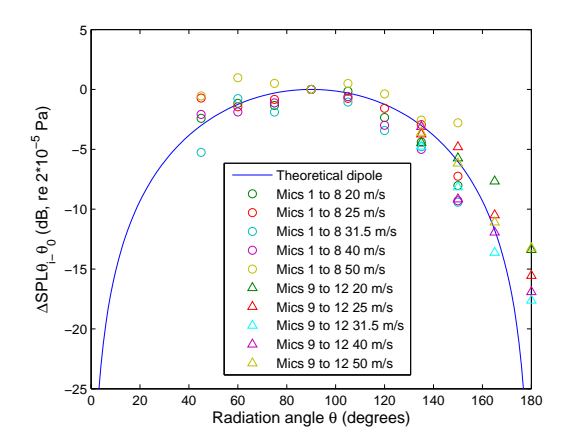


Figure 12: Directivity of vortex shedding noise measured for the right circular cylinder.

Figure 13 shows the directivity for the circular cylinder yawed by different angles for different flow speeds. Looking at the results it seems that the directivity of the vortex shedding noise is independent of the yaw angle. The dispersion increases for the higher yaw angles, mainly for the yaw angle of 75°.

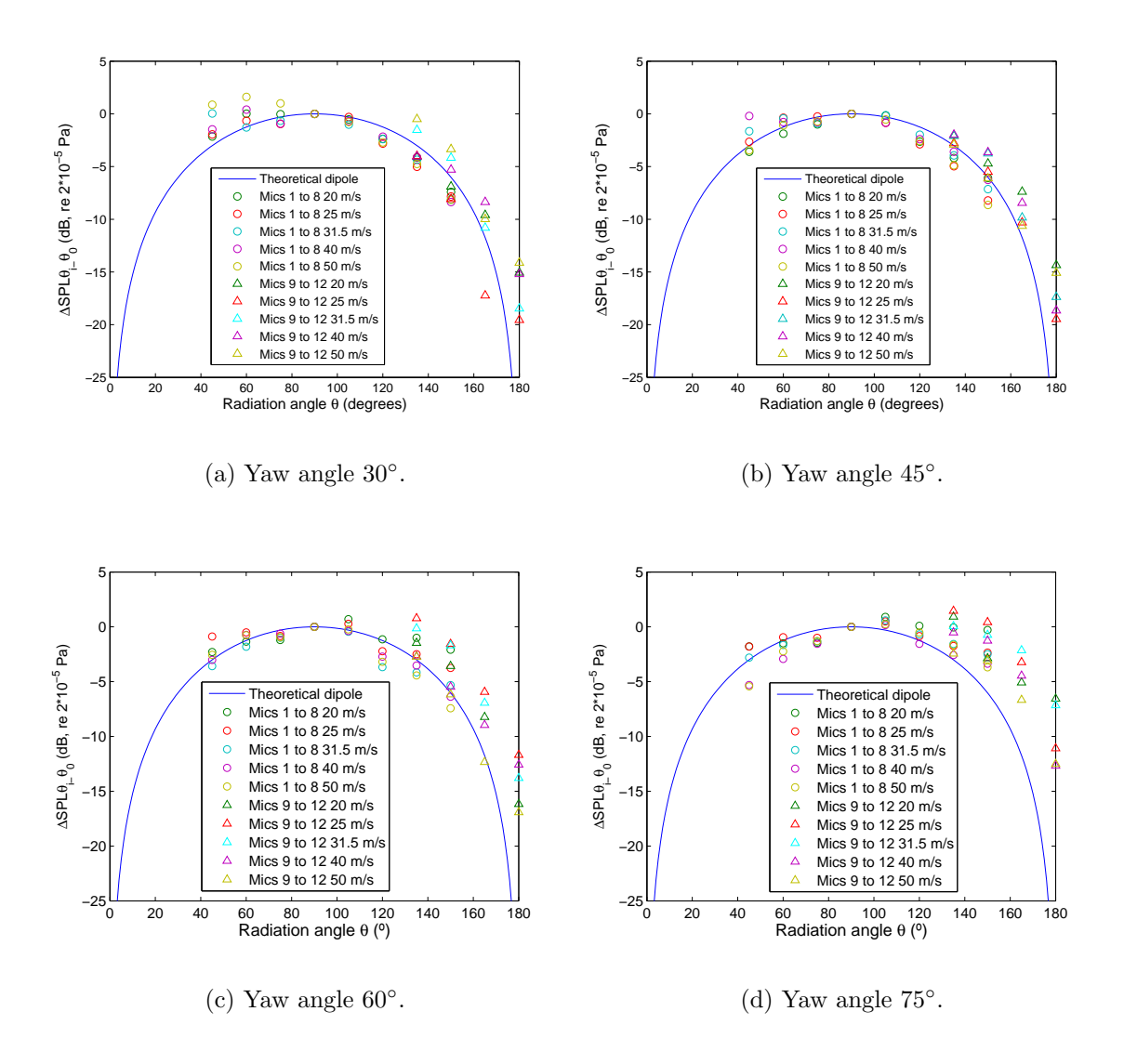


Figure 13: Directivity of vortex shedding noise measured for the circular cylinder yawed by different angles.

Figure 14 shows the narrow band noise spectrum measured by all the microphones of both arrays for the case of the circular cylinder yawed by 75° and a flow speed of 31.5 m/s. The results from microphones 10, 11 and 12 are strongly influenced by low-frequency background noise while the vortex shedding peak does not appear in the measurement from microphone 9. This fact reduces the accuracy of the results from the transversal array.

4 Square cylinder

4.1 Noise spectra

Figure 15 shows the noise spectra measured using the square cylinder for different flow speeds and yaw angles. The vortex shedding frequency and amplitude increase with the flow speed and decrease with an increase in the yaw angle. The background noise correction and the shear layer

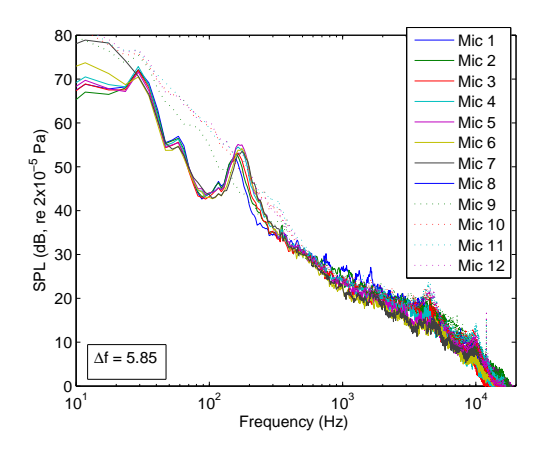


Figure 14: Narrow band noise spectrum measured by all the microphones for the case CC+Y75 and a flow speed of 31.5 m/s.

correction were not applied to the results.

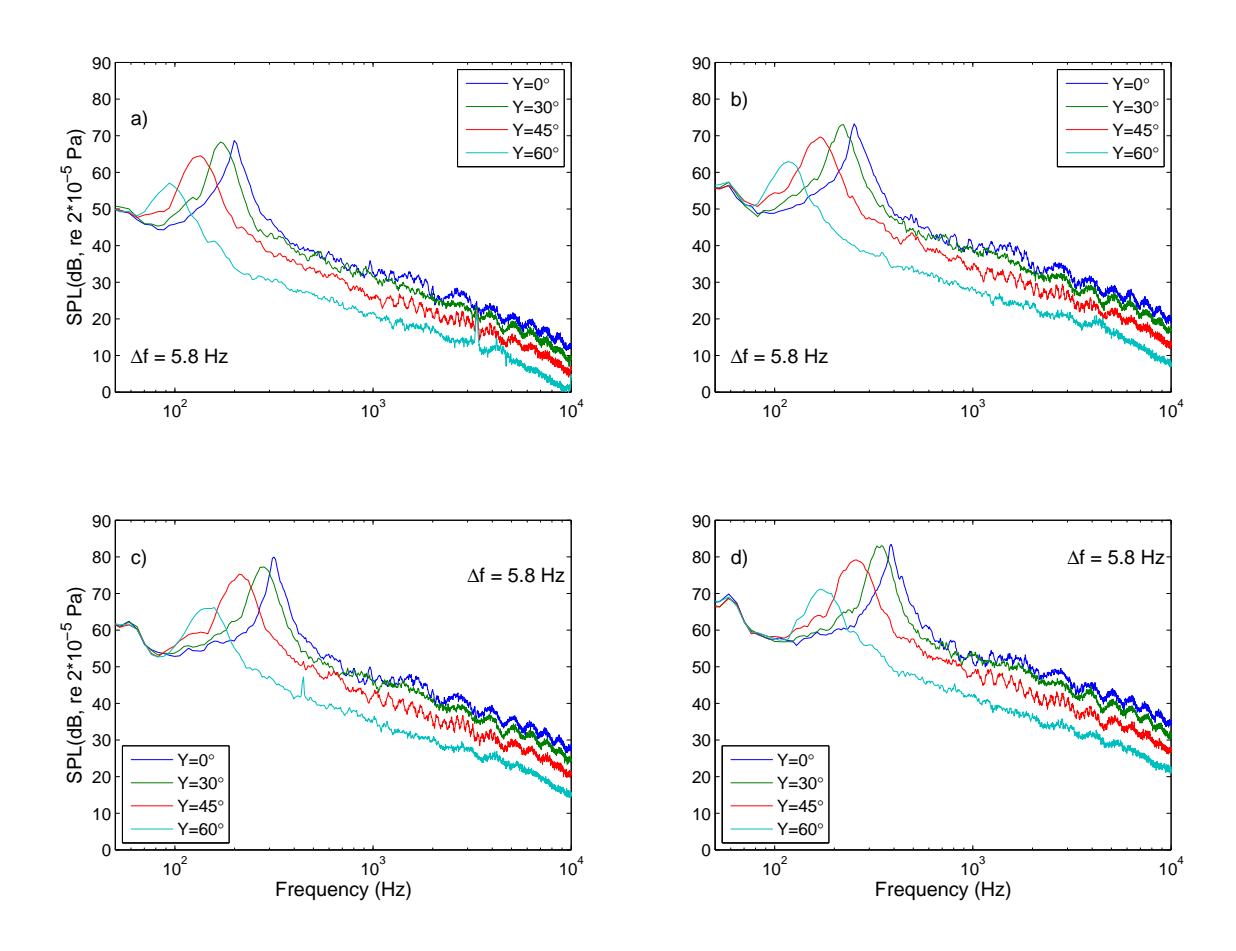


Figure 15: Narrow band noise spectra radiated by the the square cylinder for different yaw angles and flow speeds. (a) 25 m/s. (b) 31.5 m/s. (c) 40 m/s. (d) 50 m/s.

4.2 Strouhal number

The measured values of normalised Strouhal number St_n remain constant with the flow speed, as shown in Figure 16 a). The consistency in the values of the normalised Strouhal number with the flow speed shows that there is no change in the flow behaviour in the Reynolds number range evaluated.

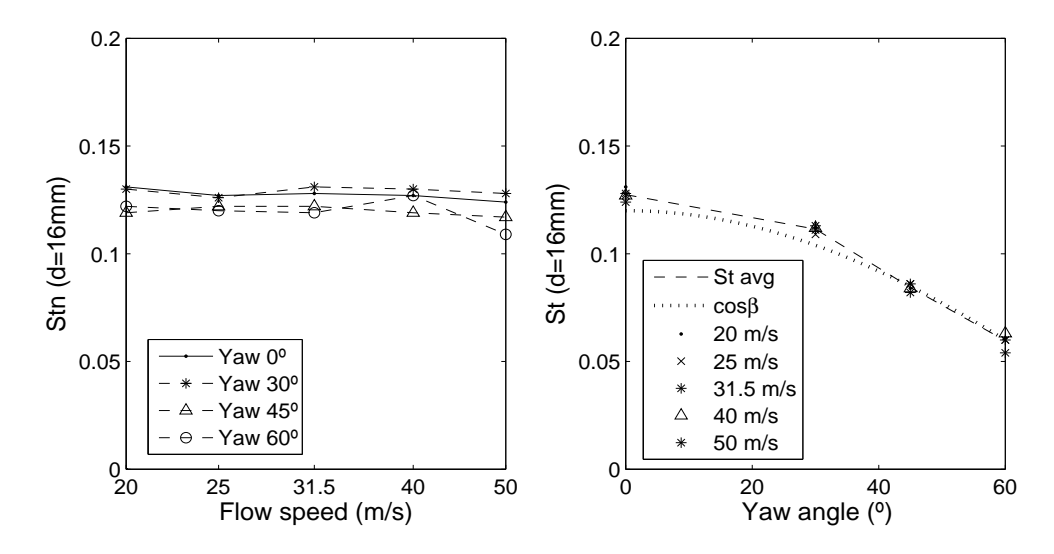


Figure 16: a) Normalised Strouhal number vs. flow speed for square cylinder. b) Variation of the Strouhal number with the yaw angle (β) . The results are compared with the factor $\cos(\beta)$.

If the variation of the Strouhal number with the yaw angle is compared to the factor $\cos(\beta)$ good agreement is obtained for all the flow speeds and yaw angles, as shown in Figure 16 b).

4.3 Amplitude of vortex shedding noise

Figure 17 shows the variation with the flow speed of the SPL in the 1/3 octave frequency band where the vortex shedding noise peak was located. The speed exponents calculated from the slope of the straight lines shown in Figure 17 are listed in Table 8. The speed exponents for the yaw angles of 30° and 45° are as expected for a dipole source but the speed exponents for the angles of 0° and 60° are slightly lower. The reason why a lower speed exponent than expected is obtained remains unknown in the case of the right cylinder and the cylinder yawed by 60° .

Table 8: Speed exponents for the square cylinder for different yaw angles.

SQUARE CYLINDER								
Yaw angles (β)	Speed exponent (α)							
0°	5.6							
30°	5.9							
45°	6.0							
60°	5.5							

The variation of the vortex shedding peak noise level with the yaw angle is shown in Figure 18. Comparing the trend followed with that defined by the factor $\cos^6(\beta)$, the noise levels for the

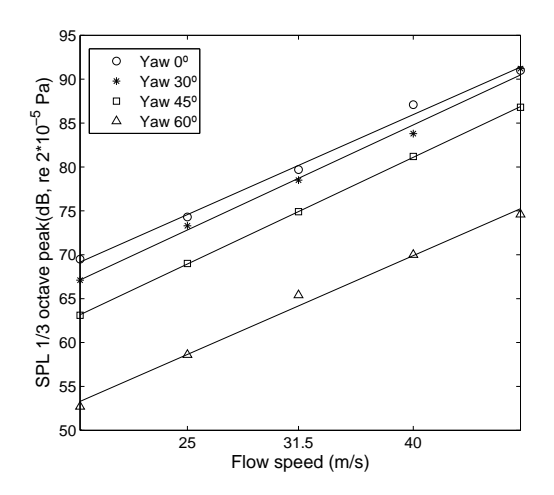


Figure 17: Variation of the SPL with the flow speed for the square cylinder.

angles of 30° and 45° are significantly higher, closer to the factor $\cos^4(\beta)$, but the result for 60° is closer to the factor $\cos^6(\beta)$.

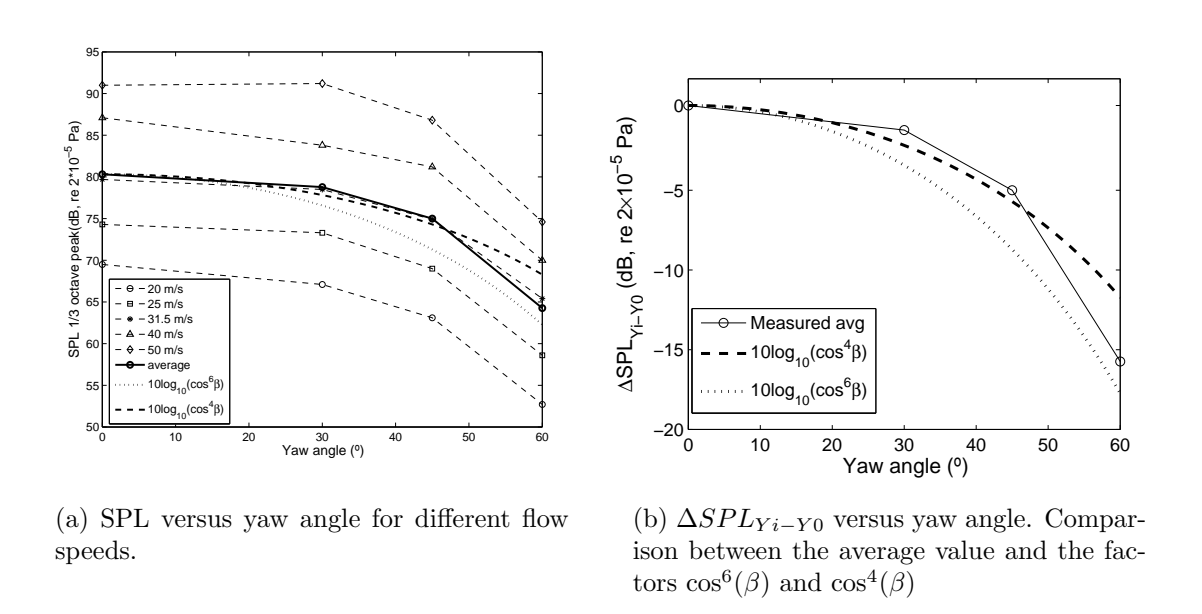


Figure 18: Variation of the SPL and ΔSPL_{Yi-Y0} with the yaw angle for a square cylinder.

4.4 Directivity of the vortex shedding noise

Figure 19 shows the noise level measured at the different radiation angles for the square cylinder for each of the flow speeds and yaw angles. The trend followed is close to the directivity pattern of a theoretical dipole, with a small dispersion in the results for the angles close to the central positions. The dispersion increases for larger angles downstream and upstream of the cylinder. The comparison between the results measured from the two different microphone arrays for the angles of 135° and 150° are in good agreement and show the symmetry of the directivity pattern. For a yaw angle of 60° the results for a flow speed of 20 m/s were not included because the vortex shedding frequency was low and consequently the vortex shedding peak was masked by

low-frequency background noise. The dispersion found for the higher angles downstream of the cylinder is about 5 dB, which is higher than for lower yaw angles.

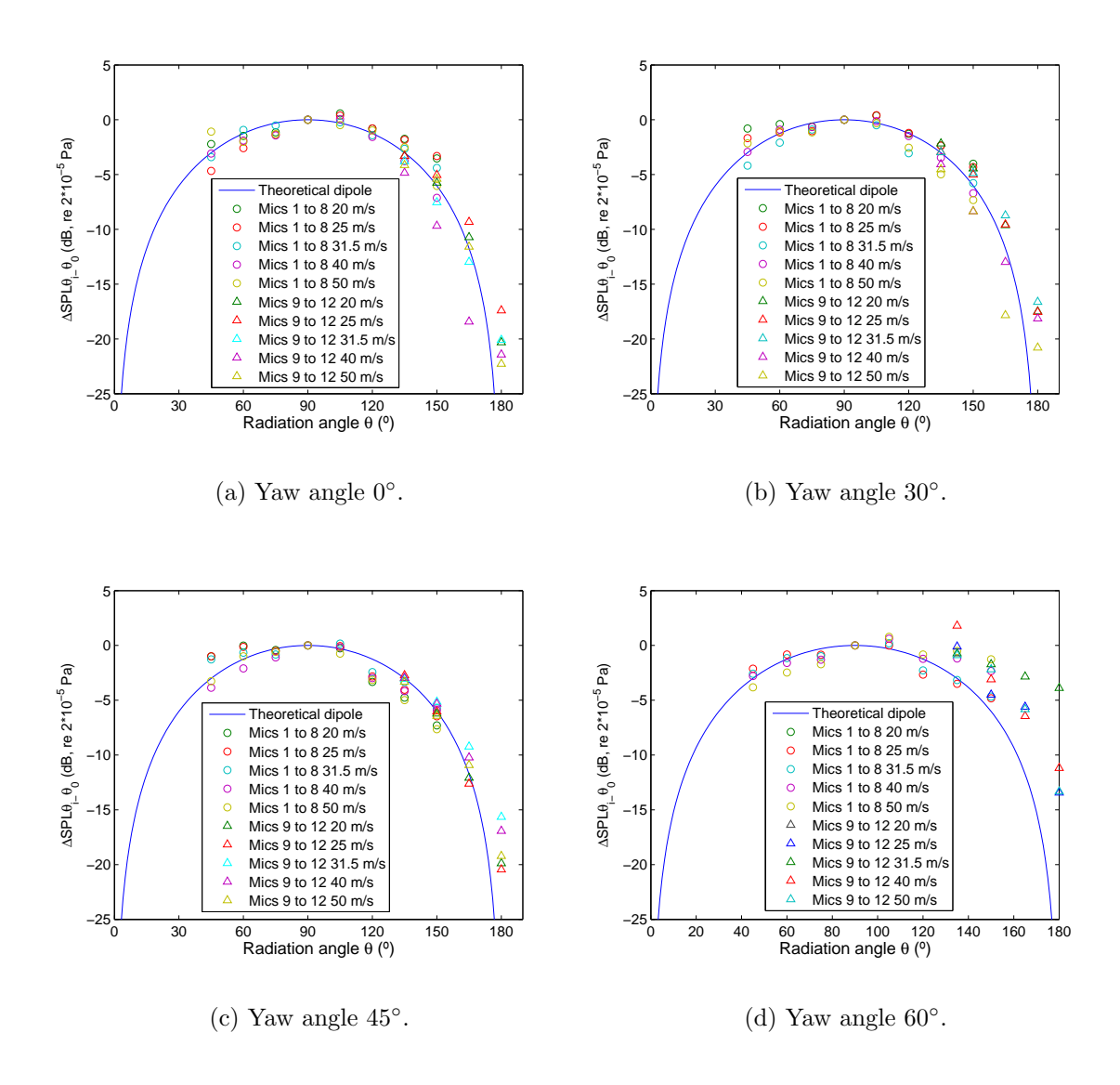


Figure 19: Directivity pattern of vortex shedding noise for a square cylinder yawed by different angles.

4.5 Angle of attack

Figure 20 shows the narrow band noise spectrum for a square cylinder at different angles of attack and flow speeds. The results show a small reduction of the vortex shedding peak amplitude when the cylinder is rotated by 10°. The decrease in the SPL is significant when the angle of attack is increased to 15°, showing that the vortex shedding is very weak at an angle of attack of 15° and is not longer triggered for larger angles so the noise spectrum is governed by broadband noise.

Figure 21 a) shows the variation of the Strouhal number with the angle of attack. The results have been averaged over the different flow speeds. The results for each individual flow speed are shown by using markers. The average Strouhal number remains constant with the angle of attack for angles below 15°. The Strouhal number for higher angles of attack is not plotted since the

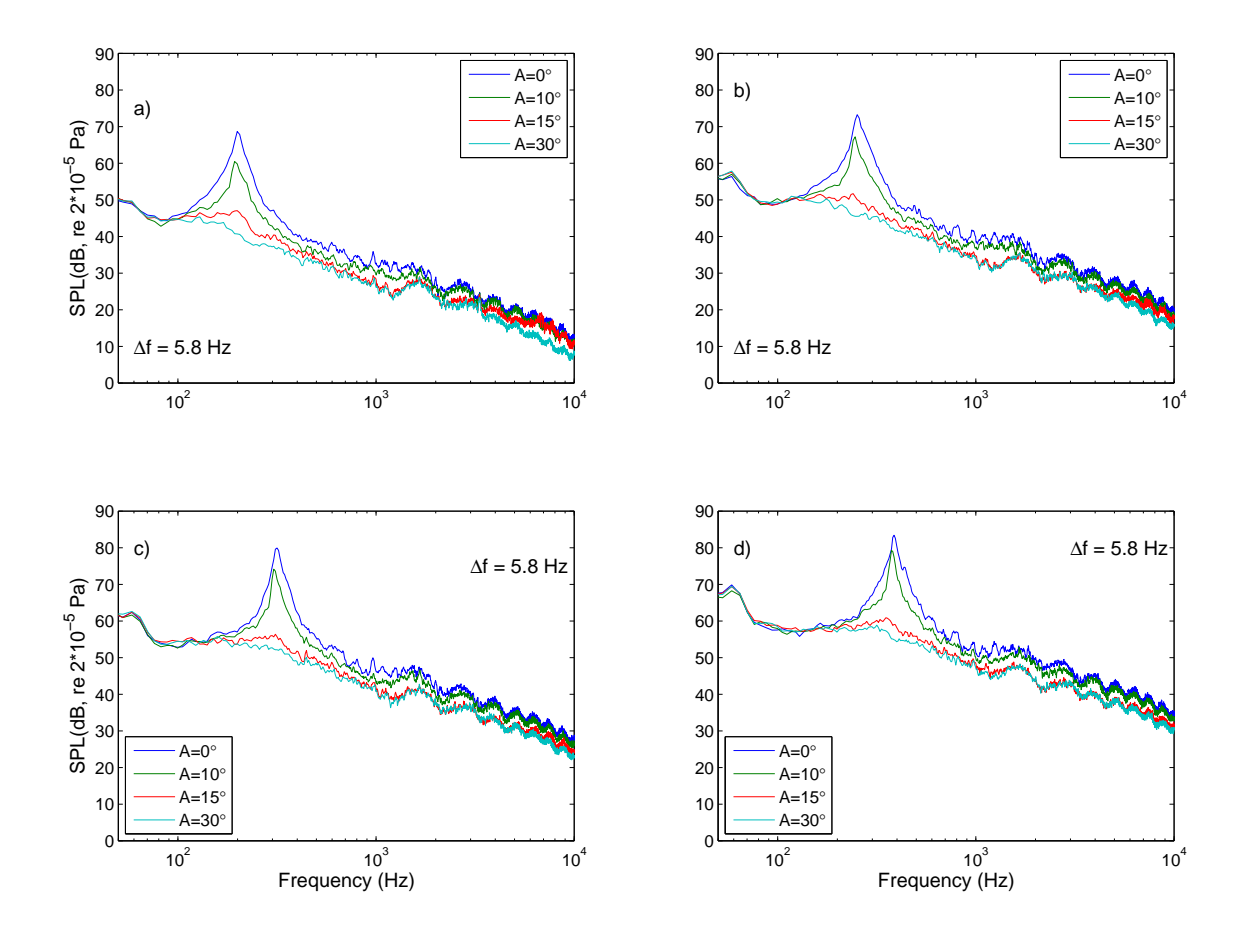


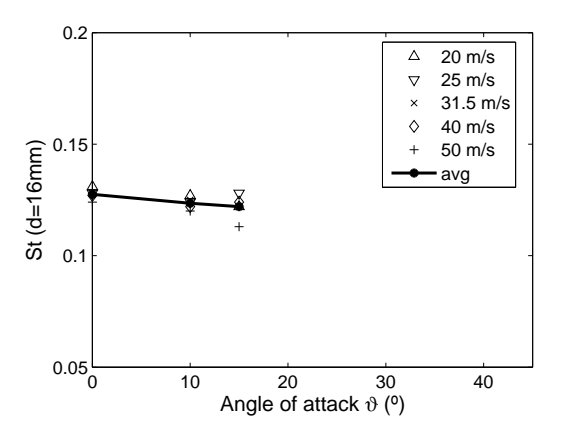
Figure 20: Narrow band noise spectra radiated by the square cylinder for different angles of attack and flow speeds. (a) 25 m/s. (b) 31.5 m/s. (c) 40 m/s. (d) 50 m/s.

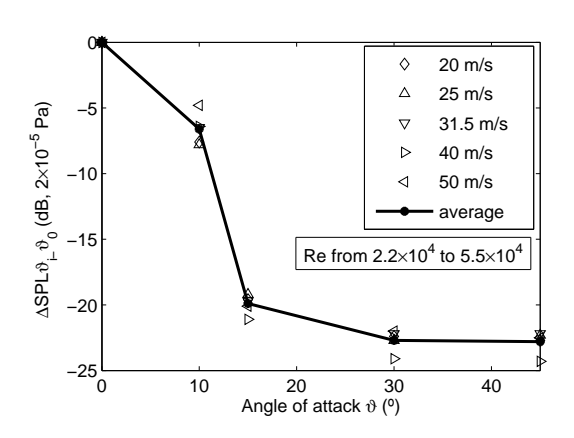
vortex shedding was not triggered. The variability of the Strouhal number with the flow speed increases for the angle of attack of 15°.

The decrease of the SPL (maximum 1/3 octave frequency band) as a function of the angle of attack ($\Delta SPL_{\vartheta_i-\vartheta_0}$, where ϑ_i is the i^{th} angle of attack and ϑ_0 is the angle of attack of 0°) is shown in Figure 21 b). As expected, the SPL decreases abruptly for angles of attack higher than 10° because the vortex shedding is no longer triggered.

Figure 22 shows the directivity pattern obtained for the square cylinder with angles of attack of 0° and 10° . Supposing a fluctuating lift force normal to the cylinder surface perpendicular to the flow direction, for an angle of attack of 10° , it might be expected that the axis of radiation of the vortex shedding noise may also be shifted by 10° . The results shown in Figure 22 do not show this effect, and the differences in the directivity between the attack angles of 0° and 10° are relatively small.

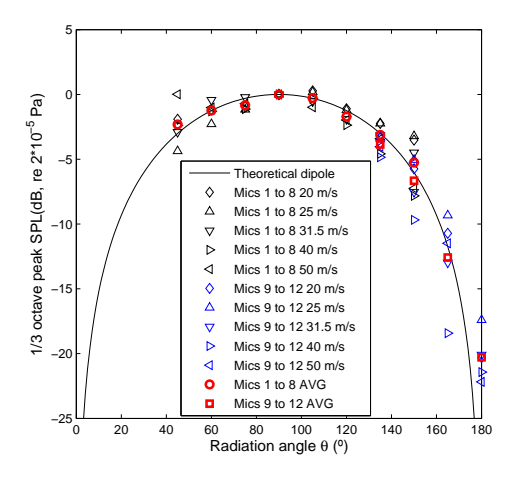
If the measured directivity pattern is compared with the theoretical directivity pattern for a dipole sound source the agreement is good in both cases. However, the dispersion in the data is considerable. The results shown are not conclusive about whether the radiation angle is shifted with the angle of attack. For angles of attack above 15° (not shown) the vortex shedding is not triggered and the directivity is nearly omnidirectional as the noise spectrum becomes broadband.





- (a) Strouhal number versus angle of attack.
- (b) Vortex shedding peak SPL decrease as a function of the angle of attack for a square cylinder with sharp edges.

Figure 21: Variation of the Strouhal number and the $\Delta SPL_{\vartheta_i-\vartheta_0}$ with the angle of attack for a square cylinder with sharp edges.



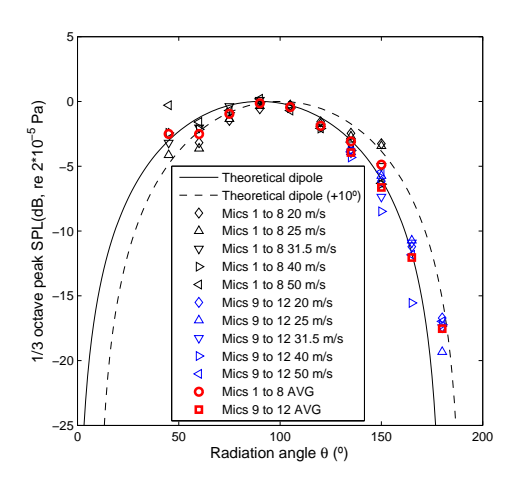


Figure 22: Comparison between the theoretical directivity pattern of a dipole source and that measured experimentally for the vortex shedding noise from a square cylinder. (a) Angle of attack (ϑ) of 0° . (b) Angle of attack (ϑ) of 10°

4.6 Square cylinder with rounded edges

Figure 23 shows the narrow band noise spectra measured using the square cylinder with rounded edges (Sr) for angles of attack of 0° , 10° and 30° and different flow speeds. The effect of varying the angle of attack of the cylinder it is different to that obtained for the square cylinder with sharp edges. For an attack angle of 10° the vortex shedding frequency increases and the amplitude of the vortex shedding peak decreases slightly, except for the flow speed of 25 m/s where the amplitude is even lower than that for the angle of attack of 0° . Nevertheless, when the angle of attack is increased to a value of 30° the vortex shedding frequency becomes higher than for 0° and 10° and the amplitude of the peak is higher than for any of the other angles.

Figure 24 shows that significant reductions of the maximum 1/3 octave band SPL are obtained when the edges of the square cylinder are rounded. The reduction obtained for a flow speed of 20

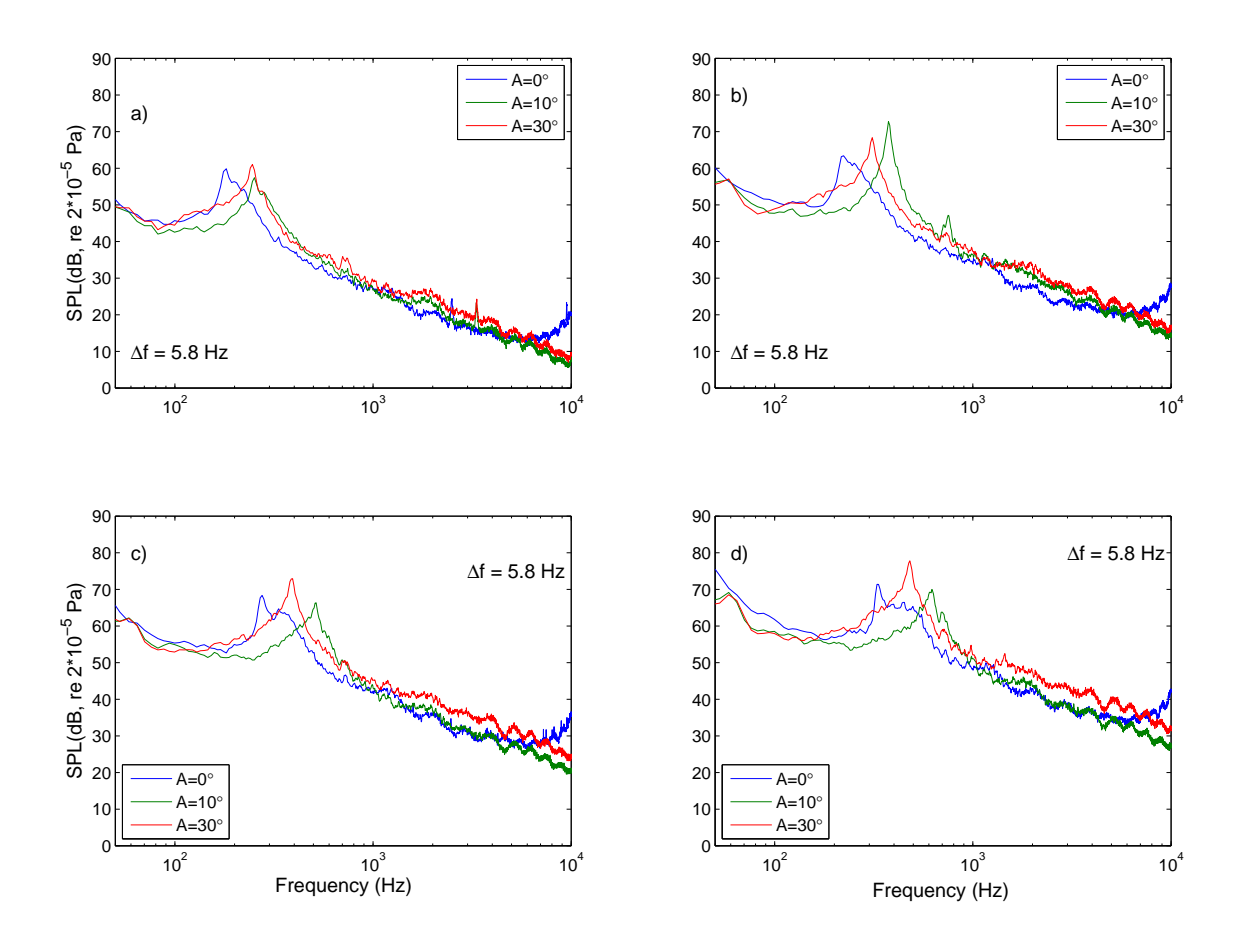


Figure 23: Narrow band noise spectra measured radiated by the square cylinder with rounded edges for different yaw angles and flow speeds. (a) 25 m/s. (b) 31.5 m/s. (c) 40 m/s. (d) 50 m/s.

m/s is 17.1 dB. Greater reductions are found as of the flow speed increases up to values of 22.8 dB for a flow speed of 50 m/s. A speed exponent of 4.1 is obtained for the square cylinder with rounded edges, significantly lower than that obtained for the cylinder with sharp edges (5.6). The noise spectrum peak is broader when the edges of the square cylinder are rounded, as can be seen by comparing the narrow band noise spectra shown in Figure 15 and Figure 23.

Figure 25 a) shows the trend followed by the Strouhal number with the angle of attack. The Strouhal number increases considerably when the cylinder is rotated by 10° and decreases slightly for an angle of attack of 30° . According to Fujita [16], sudden changes in the Strouhal number can occur due to the reattachment of the separated flow to the side faces of the square cylinder for angles between 5° and 15° , this value being dependent on the ratio r/D. In the present work the exact angle for the sudden change of St cannot be localized precisely because no more data was acquired for angles of attack between 0 and 10° .

The change in SPL from the vortex shedding noise radiated by the square cylinder with rounded edges which is rotated by the i^{th} angle of attack (A_i) relative to 0° is shown in Figure 25 b). There is a slight decrease of the SPL between the angle of attack of 0° and 10°, increasing for an angle of attack of 30°.

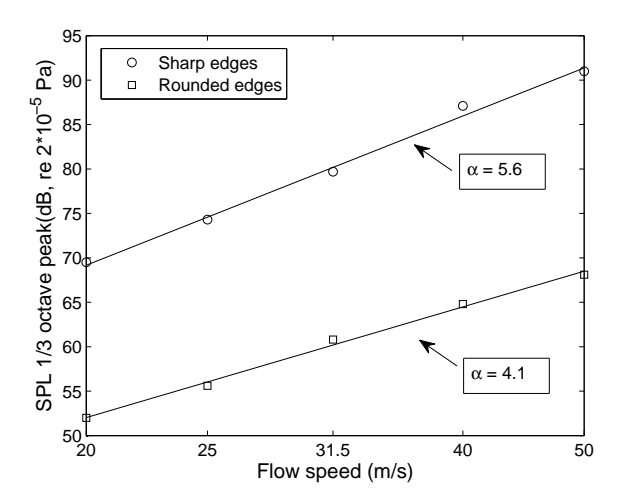


Figure 24: Variation of the maximum 1/3 octave band SPL with the flow speed for the quare cylinder with sharp and rounded edges. The speed exponents obtained for both cases are detailed.

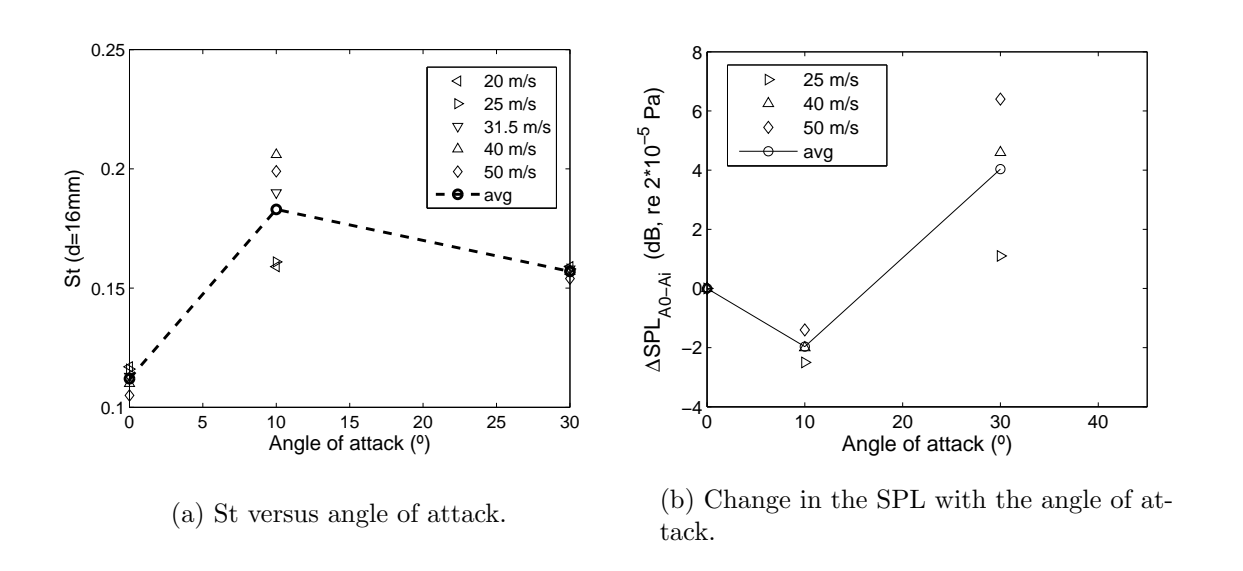


Figure 25: Variation of the Strouhal number and the SPL (peak 1/3 octave band) with the angle of attack measured for the square cylinder with rounded edges (r = D/12) at different flow speeds. The subindex A_0 refers to an angle of attack of 0° and the subindex A_i refers to the i^{th} angle of attack.

5 Rectangular cylinders

5.1 Noise spectra

Figure 26 shows the noise spectra measured for a rectangular cylinder with aspect ratio of 1.33 (R1) and different yaw angles and flow speeds. No correction is applied here for the background and shear layer noise. The amplitude and frequency of the vortex shedding peak decrease with increasing flow speed and with the increase of the yaw angle. For the yaw angle of 60° the vortex shedding peak almost vanishes and the noise spectrum is mainly broadband.

The noise spectra measured when the cylinder R1 is rotated by 90° (R1+A90), obtaining an

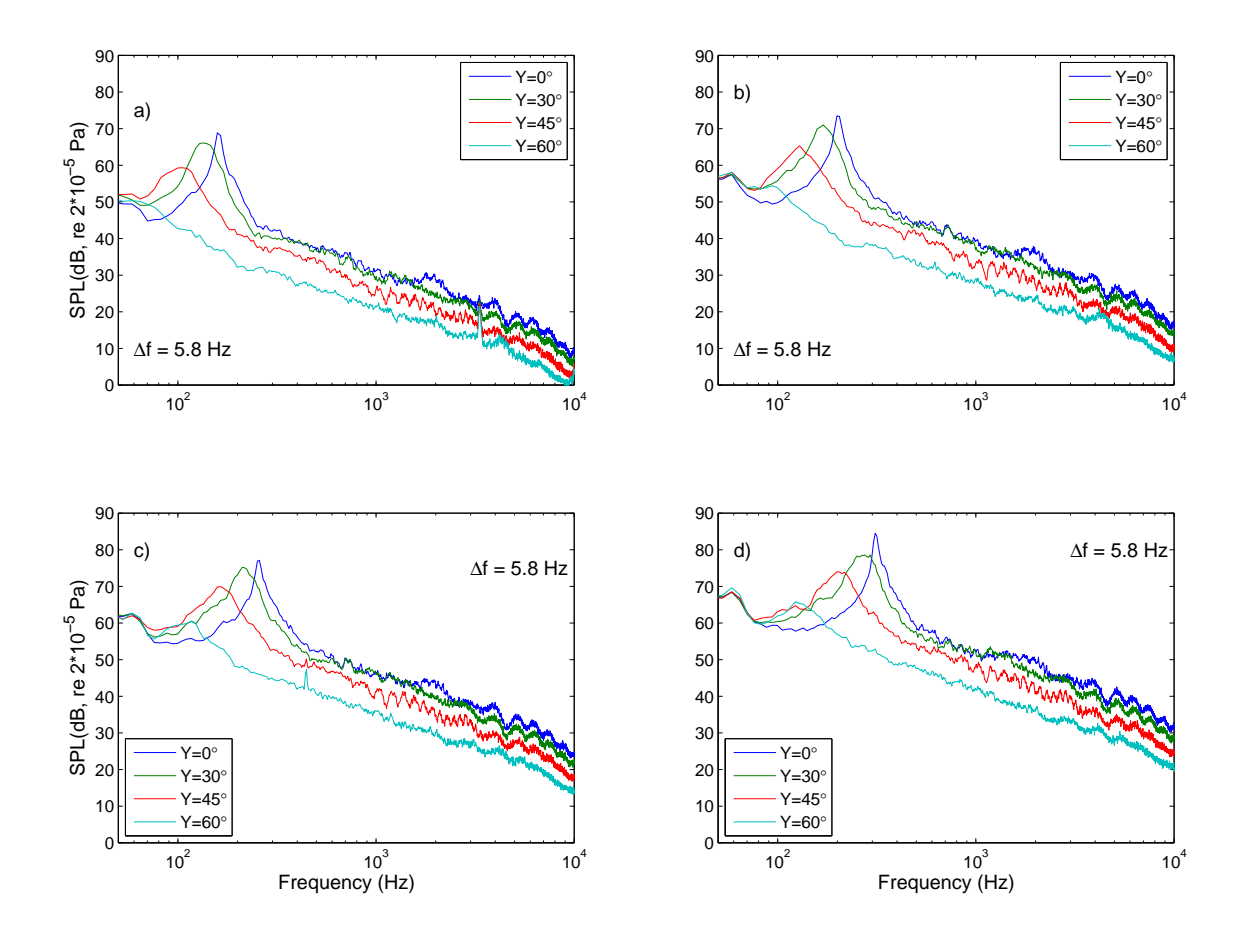


Figure 26: Narrow band noise spectra radiated by the rectangular cylinder with aspect ratio of 1.33 (R1) for different yaw angles and flow speeds. (a) 25 m/s. (b) 31.5 m/s. (c) 40 m/s. (d) 50 m/s.

aspect ratio of 0.75, is shown in Figure 27. For a yaw angles of 0° the vortex shedding was not triggered, the reason for this being unknown. For the other yaw angles tested the vortex shedding was triggered and the frequency and amplitude of the vortex shedding peak decreased when the yaw angle increased or the flow speed decreased.

Figure 28 shows the noise spectra measured using a rectangular cylinder of aspect ratio L/D=2 with an angle of attack of 0° (R2) and 90° (R2+A90, obtaining an aspect ratio L/D=0.5) for different flow speeds. The vortex shedding frequency and amplitude increase with the flow speed. The cylinder R2 was not tested for other yaw angles.

5.2 Strouhal number

Figure 29 a) shows the variation of normalised Strouhal number St_n with the flow speed for the test cases R1 and R1+A90. The normalised Strouhal number for the cylinder R1 does not vary with the flow speed or the yaw angle, St_n being between 0.10 and 0.12, except for the yaw angle of 60° and the flow speeds of 20 and 50 m/s, for which the variability is higher. In the case of the cylinder R1+A90, St_n is based on the larger dimension of 23.3 mm. Nevertheless it is slightly

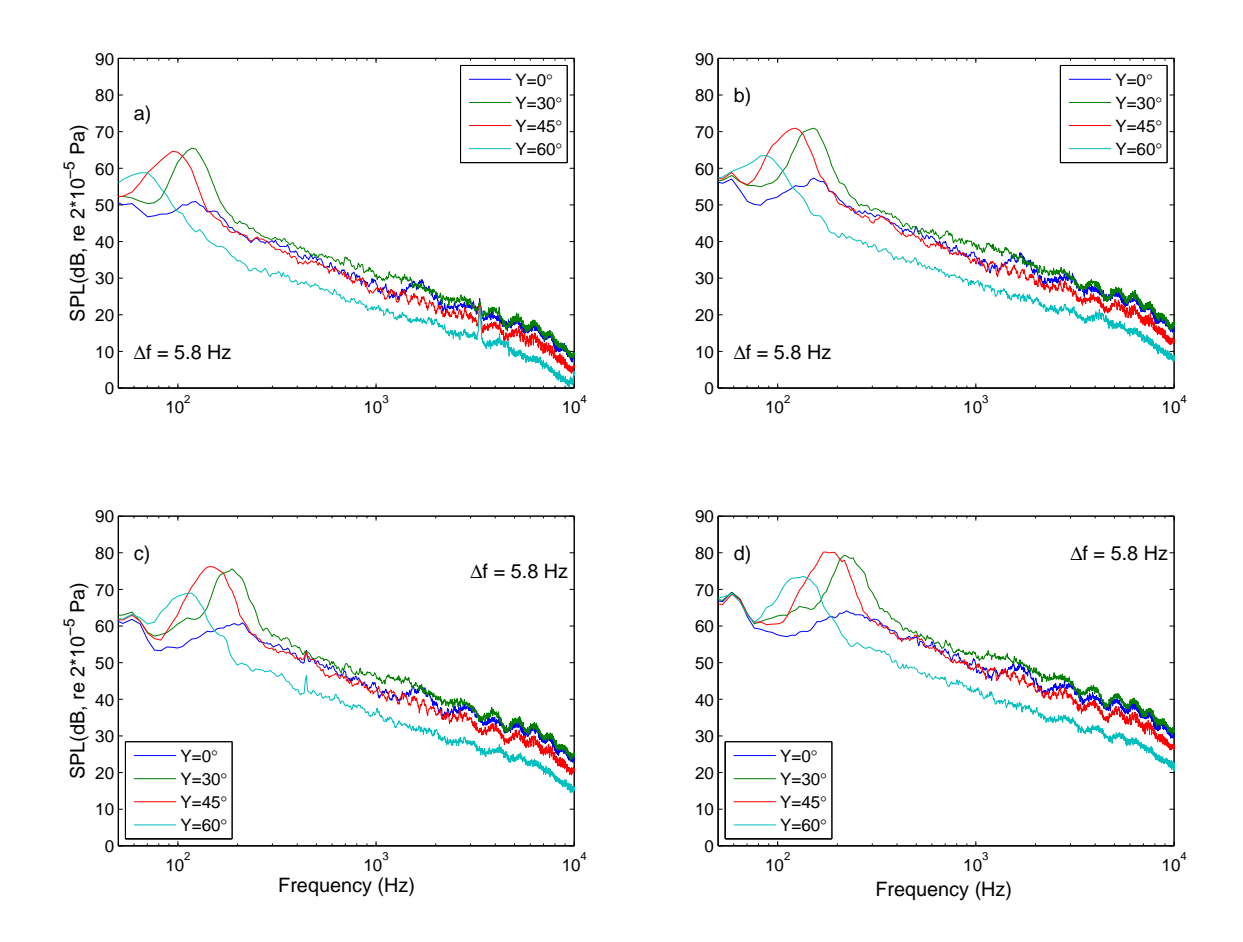


Figure 27: Narrow band noise spectra radiated by the rectangular cylinder with aspect ratio of 0.75 (R1+A90) for different yaw angles and flow speeds. (a) 25 m/s. (b) 31.5 m/s. (c) 40 m/s. (d) 50 m/s.

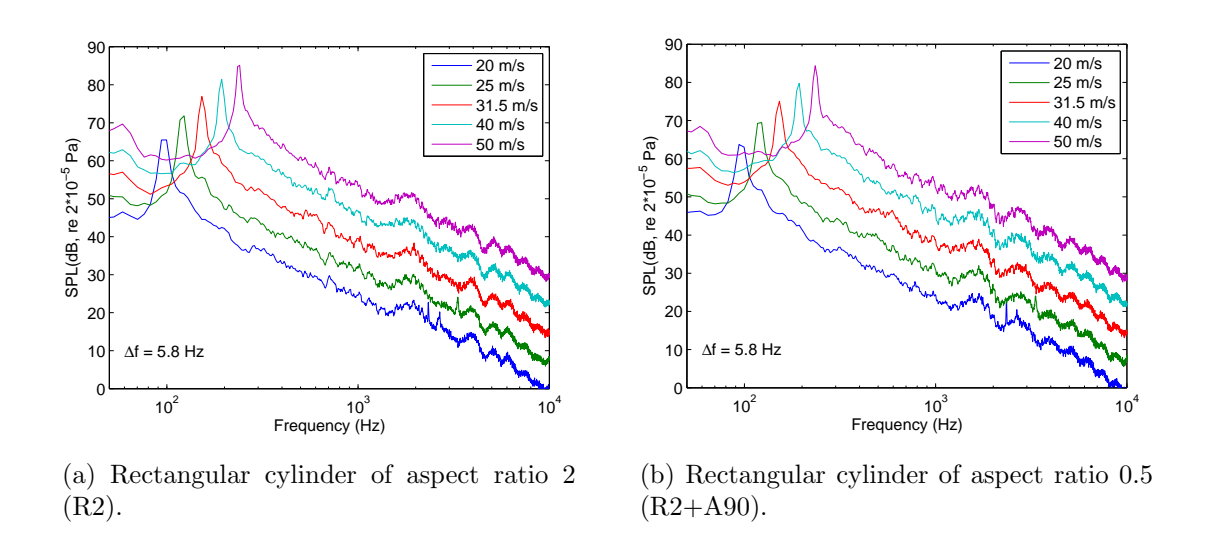
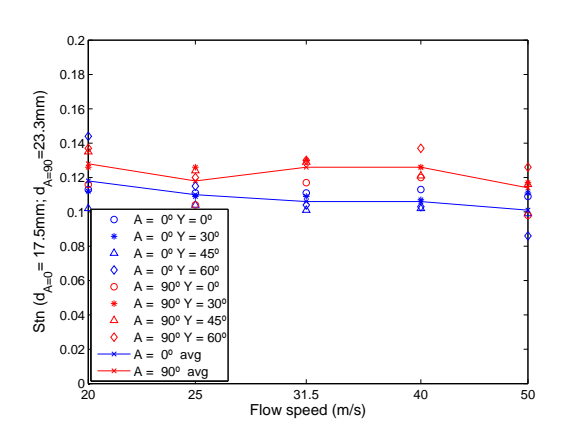
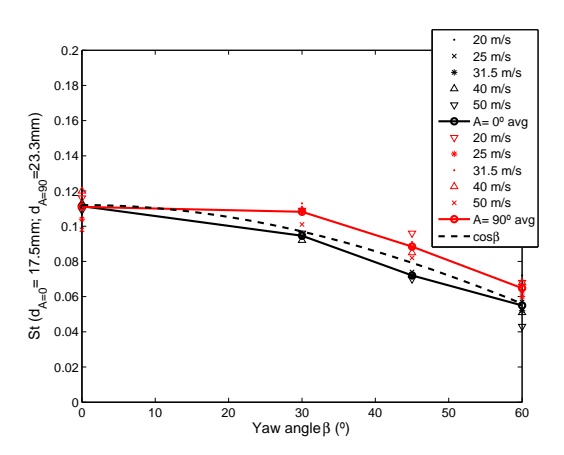


Figure 28: Narrow band noise spectrum for the right rectangular cylinders R2 and R2+A90.

higher than for the cylinder R1 and the variability is also higher, with values around 15%.

Figure 29 b) shows the variation of St with yaw angle for the cylinders R1 and R1+A90. In both cases a good agreement is found between the trend followed by the average St measured and the theoretical factor $\cos \beta$ derived from the independence principle.





- (a) St_n versus flow speed for different yaw angles.
- (b) St versus yaw angle for different flow speeds. Comparison with the factor $\cos(\beta)$.

Figure 29: Variation of St_n with the flow speed and St with the yaw angle for the rectangular cylinders with aspect ratio 1.33 (R1) and 0.75 (R1+A90).

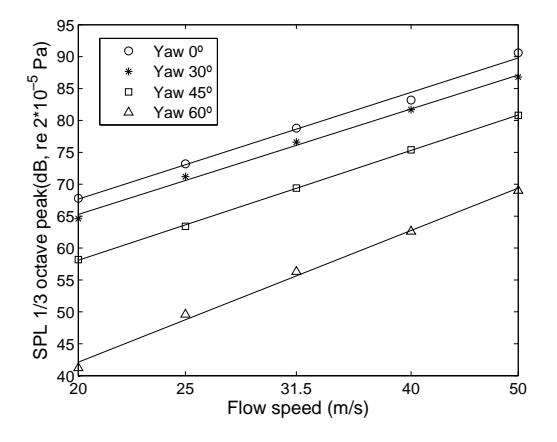
Table 9 shows the values of the St obtained for the right rectangular cylinders R2 and R2+A90. The Strouhal number for the cylinder R2 is significantly lower than the values obtained for the other rectangular cylinders considered and it seems to be independent of the flow speed in the Reynolds number range covered. The Strouhal number increases noticeably when the cylinder R2 is rotated by 90° and it is again nearly independent of the flow speed.

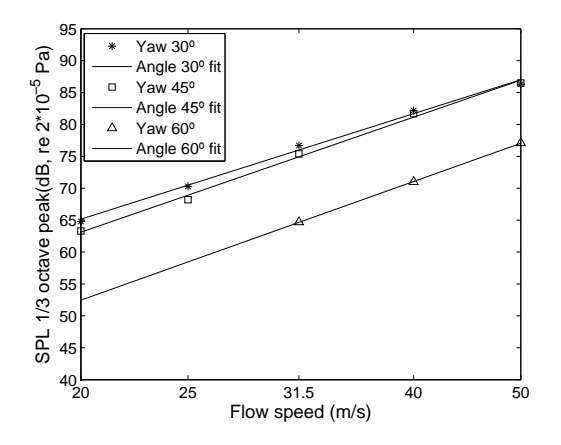
Table 9: St for the right rectangular cylinders with aspect ratio 2 (R2) and 0.5 (R2+A90) for different flow speeds, based on the characteristic dimension D of 17.5 mm (R2) and 35.0 mm (R2+A90).

		Flow speed (m/s)							
		20	25	31.5	40	50			
_	-	0.087							
R	R2+A90	0.164	0.172	0.169	0.169	0.164			

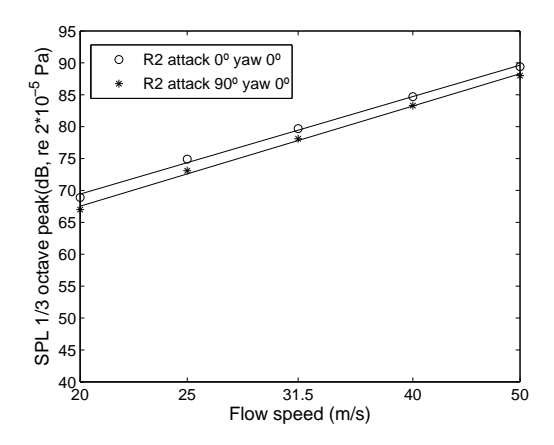
5.3 Amplitude of the vortex shedding noise

Figure 30 shows the variation of the peak 1/3 octave band SPL with the flow speed for the different rectangular cylinders with aspect ratio of 1.33, 0.75, 2 and 0.5. The vortex shedding was not triggered for the right cylinder R1+A90 so the results for this case are not included in Figure 30. The slope of the straight lines obtained after applying linear curve fitting to the results shown in Figure 30 gives the speed exponents for the different rectangular cylinders, as shown in Table 10. They are mostly between 5 and 6 except for the yaw angle of 60°.





- (a) Rectangular cylinder with aspect ratio of 1.33 (R1).
- (b) Rectangular cylinder with aspect ratio of 0.75 (R1+A90).



(c) Rectangular cylinders with aspect ratio of 2 (R2) and 0.5 (R2+A90).

Figure 30: Variation of the peak 1/3 octave band SPL with the flow speed for the rectangular cylinders yawed by different angles.

5.4 Directivity of the vortex shedding noise

The directivity obtained for the cylinder R1 matches that from a theoretical dipole source with differences smaller than 1 dB except for the angle of radiation of 60° for which the noise measured is around 3 dB lower, as shown in Figure 31 a). The agreement is less good for the rectangular cylinder with aspect ratio of 2. The peak level measured is slightly higher than that expected for the positions upstream of the cylinder and lower for the positions downstream of the cylinder in the case of the longitudinal array. Nevertheless, the agreement is good for the measurements made with the longitudinal array.

Table 10: Speed exponents for rectangular cylinders with different aspect ratios yawed by different angles.

	Speed exponent								
Yaw angles	R1 A=0°	R1 A=90°	R2	$R2 A=90^{\circ}$					
0	5.6	*	5.1	5.2					
30	5.5	5.5	*	*					
45	5.7	5.9	*	*					
60	6.9	6.2	*	*					

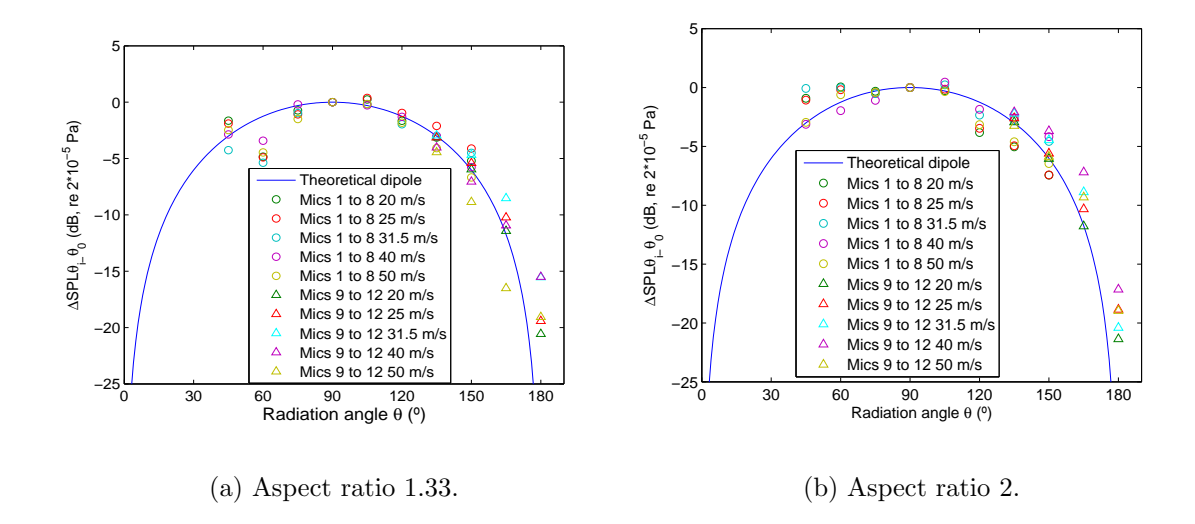


Figure 31: Directivity pattern of vortex shedding noise for a right rectangular cylinder.

6 Elliptical cylinders

6.1 Noise spectra

Figure 32 shows the narrow band noise spectra obtained for the elliptical cylinder with eccentricity e=0.63 (E1) for different flow speeds and yaw angles. The amplitude of the vortex shedding peak is, for most of the flow speeds, higher for the yaw angle of 30° than for the right cylinder. At some speeds (25 and 31.5 m/s) even the amplitude of the noise for a yaw angle of 45° is higher than for the right cylinder. A similar trend is found for the cylinder with eccentricity 0.75 (E2), as shown in Figure 33. In this case, the vortex shedding is barely triggered when the cylinder is perpendicular to the flow. In both cases a significant decrease of the peak level is obtained for yaw angles of 60°.

6.2 Strouhal number

Figure 34 a) shows the variation of normalised Strouhal number St_n with the flow speed for different yaw angles for the cylinders E1 and E2. There is no a consistent trend of the variation of St_n with the flow speed and a large variability is found in the results. Figure 34 b) shows a good

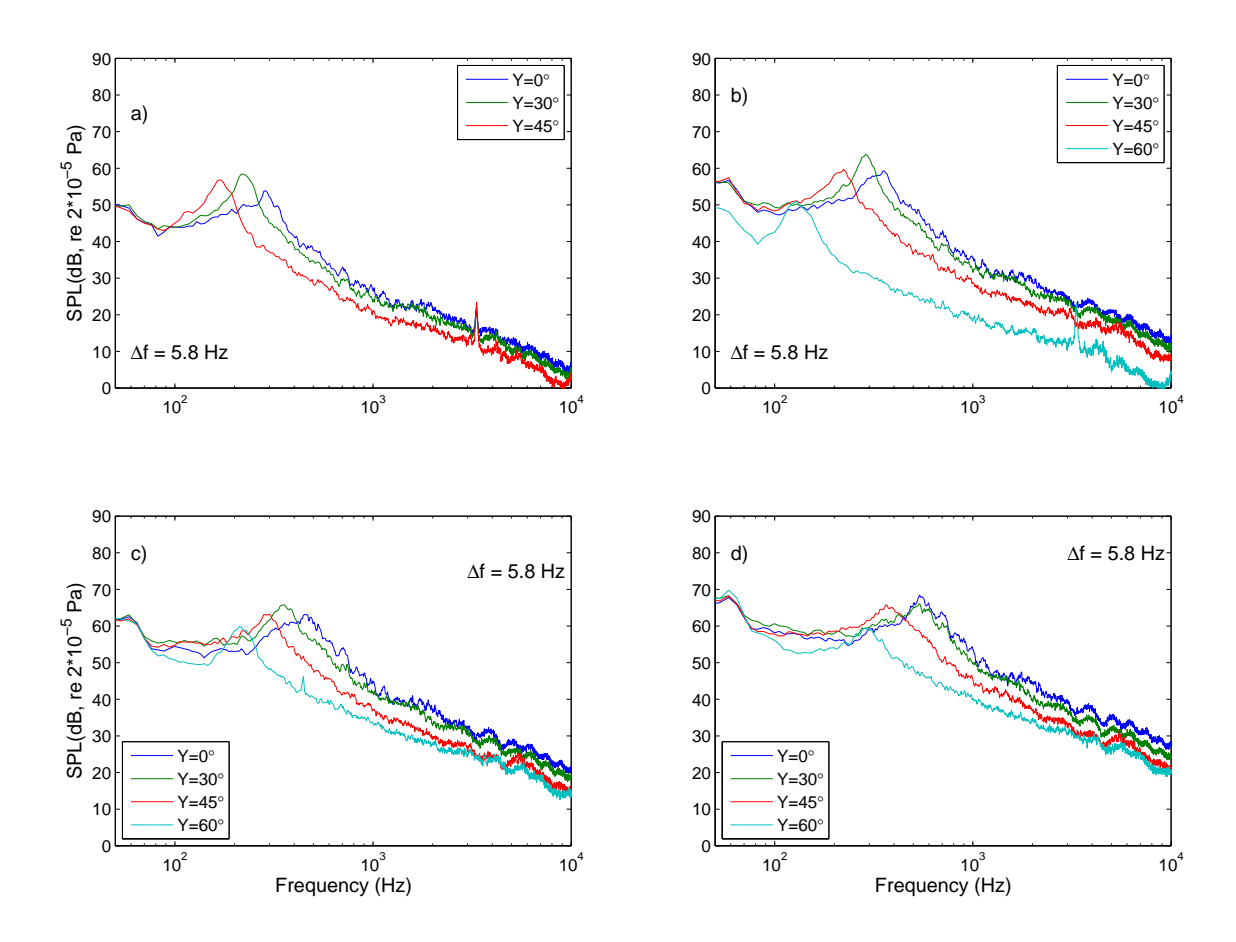


Figure 32: Narrow band noise spectra radiated by the elliptical cylinder with eccentricity of 0.63 (E1) for different yaw angles and flow speeds. (a) 25 m/s. (b) 31.5 m/s. (c) 40 m/s. (d) 50 m/s.

agreement between the variation of St with the yaw angle for the cylinders E1 and E2 when the results are compared with the theoretical factor $\cos\beta$.

6.3 Amplitude of vortex shedding noise

Figure 35 shows the variation of the maximum 1/3 octave band SPL with the flow speed for the elliptical cylinders yawed by different angles. The slope of the resultant straight line after applying linear curve fitting gives the speed exponents listed in Table 11. For the elliptical cylinder with eccentricity 0.63 (E1), the speed exponent for a yaw angle of 0° matches the theoretical speed exponent for a dipole source but for higher yaw angles the speed exponents are significantly lower. For the elliptical cylinder with eccentricity 0.75, the speed exponents for the yaw angles of 30° and 45° seem to be too high compared with the speed exponent expected for a dipole source. The fact that the peaks in the noise spectra are not very distinct in some cases makes these results less accurate.

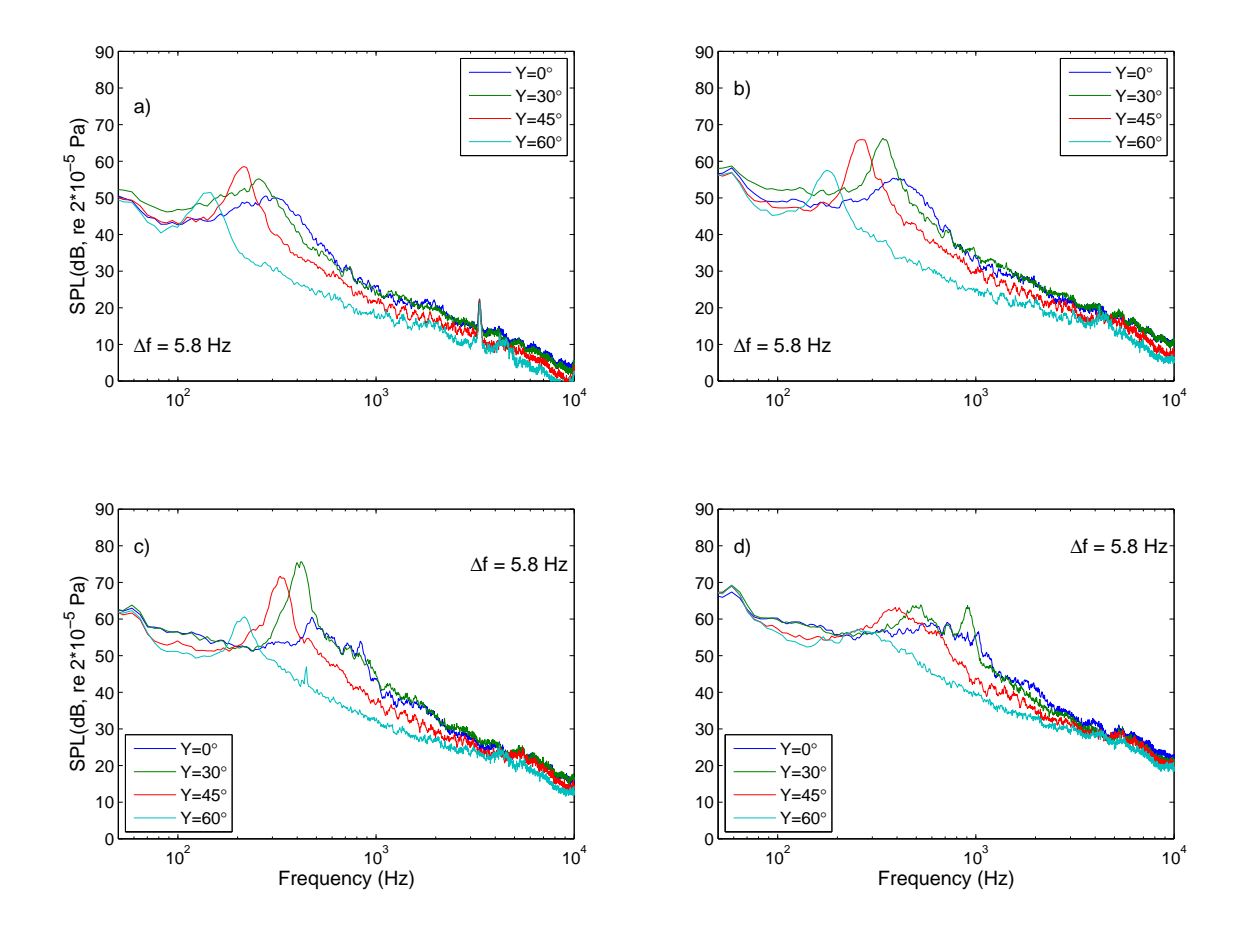


Figure 33: Narrow band noise spectra radiated by the elliptical cylinder with eccentricity of 0.75 (E2) for different yaw angles and flow speeds. (a) 25 m/s. (b) 31.5 m/s. (c) 40 m/s. (d) 50 m/s.

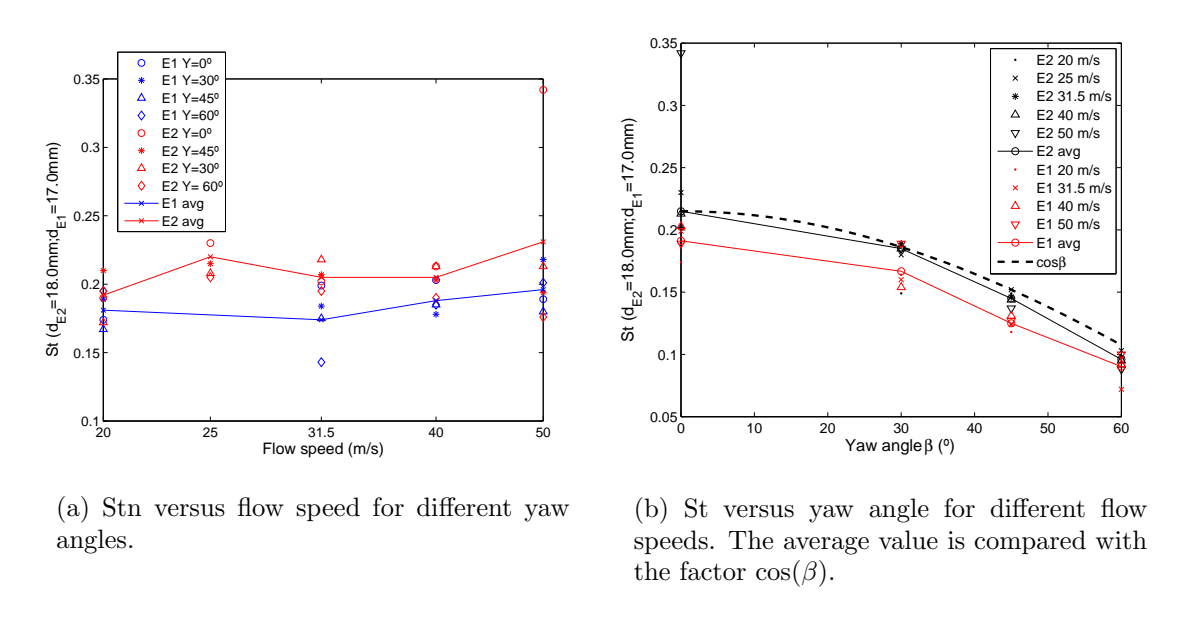
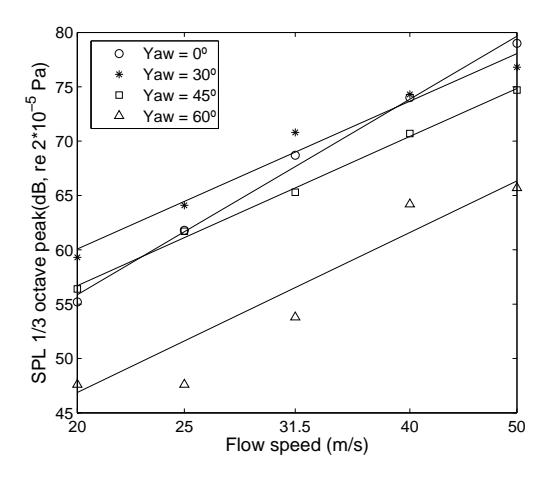
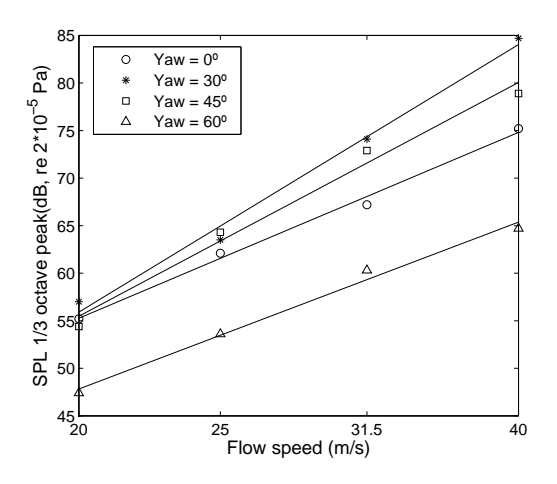


Figure 34: Variation of St_n with the flow speed and variation of St with the yaw angle for the elliptical cylinders E1 and E2.





- (a) Elliptical cylinder with eccentricity of 0.63 (E1).
- (b) Elliptical cylinder with eccentricity of 0.75 (E2).

Figure 35: Variation of the maximum 1/3 octave band SPL with the flow speed for the elliptical cylinders yawed by different angles.

Table 11: Speed exponent for different yaw angles. Elliptical cylinders with eccentricities of 0.63 (E1) and 0.75 (E2).

	Speed exponent				
Yaw angles	$\mathbf{E1}$	$\mathbf{E2}$			
0°	6.0	6.0			
30°	4.5	8.2			
45°	4.6	9.4			
60°	4.9	5.9			

6.4 Directivity of the vortex shedding noise

Figure 36 a) shows the directivity measured for the elliptical cylinder E1 in the 1/3 octave band where the vortex shedding peak was located. The directivity for all the flow speeds is represented with markers. These results are compared with the directivity for a theoretical dipole source showing a good agreement. Nevertheless, for the radiation angles of 45° and 120° differences of around 2-3 dB are found between the measurements and the theoretical values. A good agreement is found if the results from the two different microphone arrays are compared (for 135° and 150°) showing the symmetry in the noise radiation.

Similar results were obtained for the elliptical cylinder with eccentricity of 0.75. A good agreement is found in the comparison with the theoretical values except for the angles of 45° and 60°. At these angles the dispersion is higher and differences up to 5 dB are found between the measured and the theoretical values.

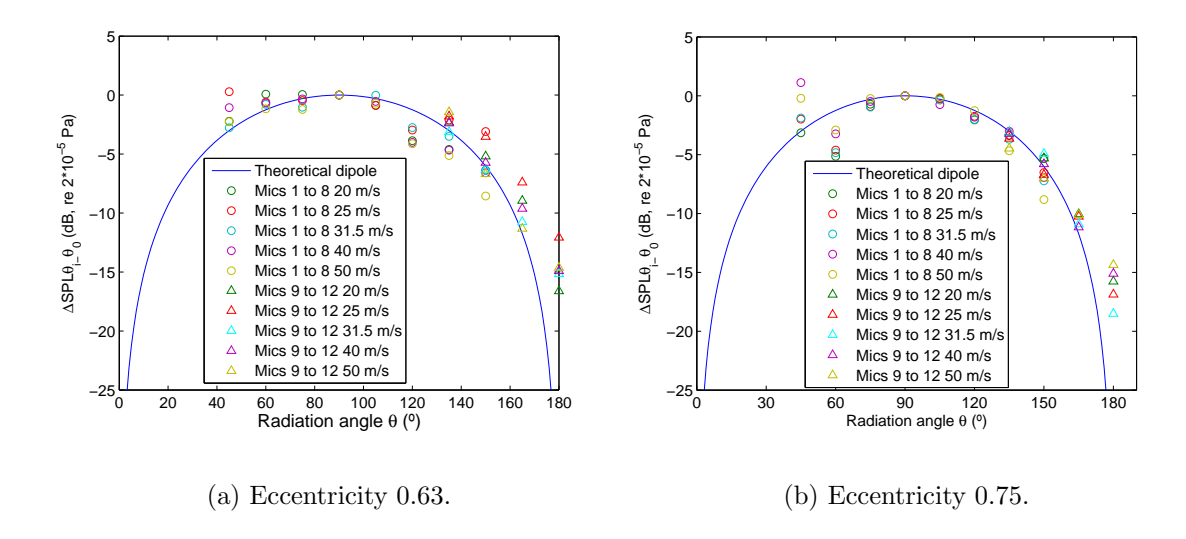


Figure 36: Directivity pattern for right elliptical cylinders.

7 Broadband noise

The recently applied semi-empirical models for the prediction of the aerodynamic noise produced by a high-speed train pantograph include not only the peak of the vortex shedding noise produced by the pantograph struts but also the broadband noise generated by them [17]. Some results obtained on the broadband noise produced by the cylinders used during the wind tunnel tests are therefore included in this report so they can be used for the modelling of the broadband noise produced by, for example, a high-speed train pantograph.

The data were processed in a similar way to that done for the vortex shedding peak noise earlier in this report. Broadband noise (hereafter called broadband SPL) is defined here as the noise for frequencies above the vortex shedding frequency, starting from the first frequency band that was found not to be influenced by the peak noise. By comparing the decreasing slope (with frequency) of the vortex shedding peak noise with the decreasing slope of the noise in the higher frequency bands, the lowest frequency band of the broadband noise range was determined. Then, the broadband noise frequency range was extended up to the highest frequency measured (20 kHz). An example of this process to choose the lower limit of the broadband noise frequency range is provided in Figure 37.

The noise for frequencies lower than the vortex shedding frequency has been neglected because, in most cases, the signal-to-noise ratio is not high enough or the frequency of the vortex shedding peak is too close to the lower limit of the frequency range, as shown in Figure 37 for the circular cylinder yawed by 60° .

7.1 Amplitude

Figure 38 a) shows the variation of the broadband SPL with the flow speed for the circular cylinder as well as the trend obtained by applying linear curve fitting. The slopes of the straight lines are different for the different yaw angles. Those slopes are taken as the speed exponents and listed in

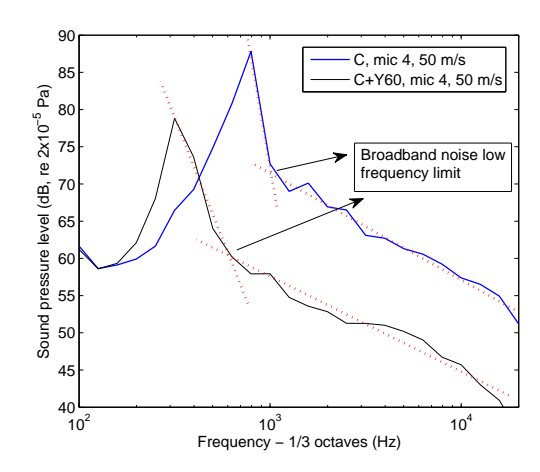


Figure 37: Examples of narrow band noise spectra for the circular cylinder with yaw angles of 0° and 60° for a flow speed of 50 m/s. The decreasing slopes for the vortex shedding peak and high-frequency broadband noise are shown. The low frequency limit of the broadband noise is chosen as the frequency of the 1/3 octave band at the intersection of both lines.

Table 12. Figure 38 b) shows the variation of the broadband SPL with the yaw angle for a circular cylinder. The decreasing slope is very similar for all the flow speeds and differs considerably from the theoretical factor of $60 \log_{10}(\cos(\beta))$.

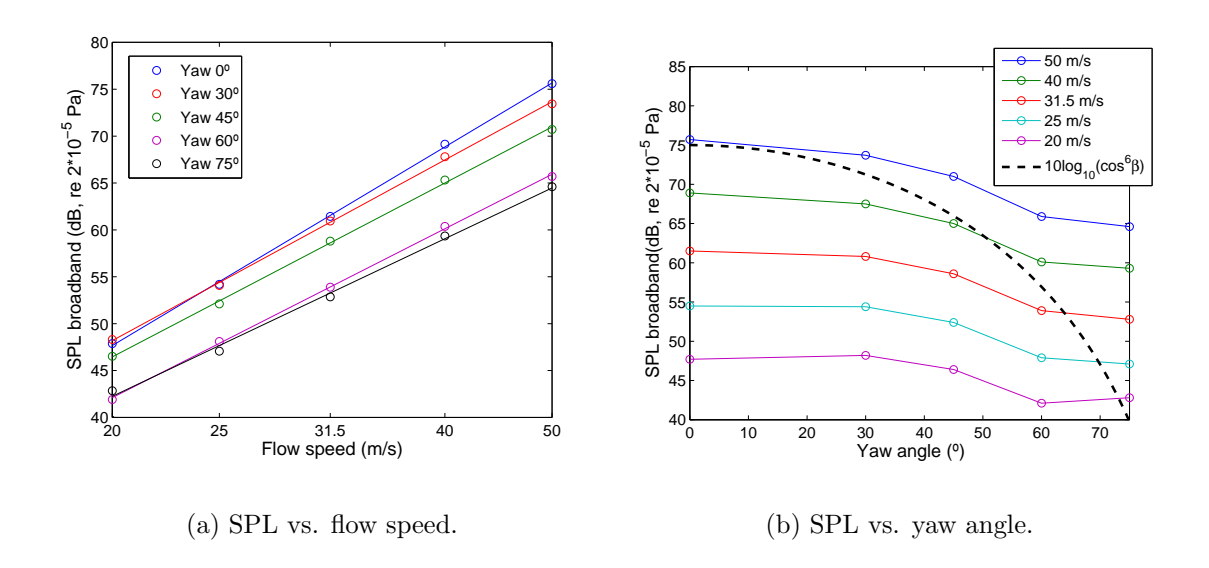


Figure 38: Variation of the broadband SPL with the flow speed and the yaw angle for a circular cylinder.

Figure 39 a) shows the corresponding results for the square cylinder. This shows a greater similarity in the increasing slopes for the different yaw angles for the square cylinder compared with the results obtained for the circular cylinder. However, the slope obtained for the yaw angle of 30° does not follow the same trend as the slopes for the other yaw angles. The variation of the SPL with the yaw angle is similar for all the flow speeds except for the flow speed of 20 m/s, as shown in Figure 39 b). The results again do not agree with the theoretical factor of $60 \log_{10}(\cos(\beta))$.

For the elliptical cylinder with eccentricity of 0.63, the increment of the SPL with the flow speed is also similar for all the yaw angles apart from 45° and 60°, as shown in Figure 40 a). For a yaw

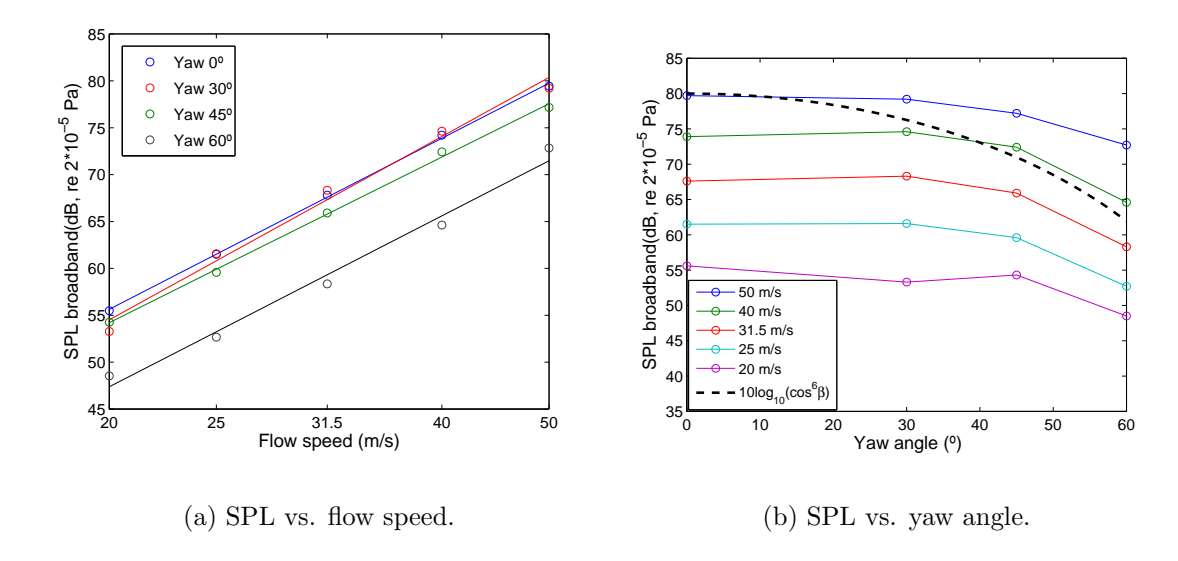


Figure 39: Variation of the broadband SPL with the flow speed and the yaw angle for a square cylinder.

angle of 60° the increase of the SPL with the increase of the flow speed does not follow a straight line trend. Figure 40 b) shows that the variation of the SPL with the yaw angle is similar for all the flow speeds for angles lower that 60° . For this angle the results depend on the flow speed. The decrease of the SPL with the yaw angle is more gradual than that obtained by the factor of $60 \log_{10}(\cos(\beta))$.

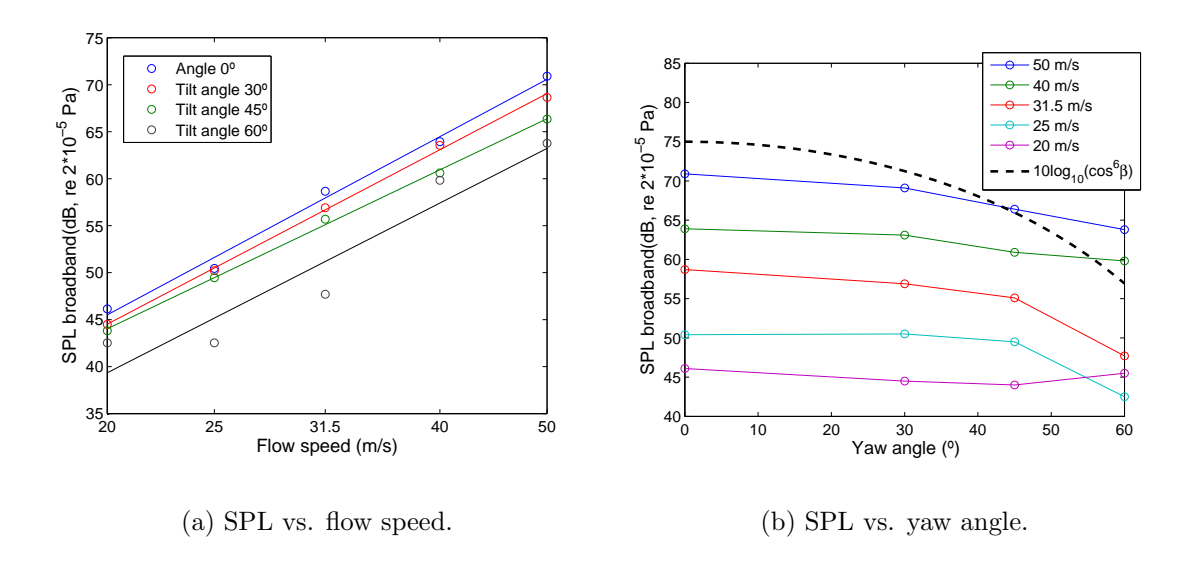


Figure 40: Variation of the broadband SPL with the flow speed and the yaw angle for the elliptical cylinder with eccentricity 0.63.

For the elliptical cylinder with eccentricity of 0.75, Figure 41 a) shows a strong disagreement between the slope for the yaw angle of 0° and the slopes obtained for other yaw angles. The trend followed for the variation of the SPL with the yaw angle also depends on the flow speed, as shown in Figure 41 b).

For the rectangular cylinder with aspect ratio of 1.33, Figures 42 a) and 42 b) show consistent

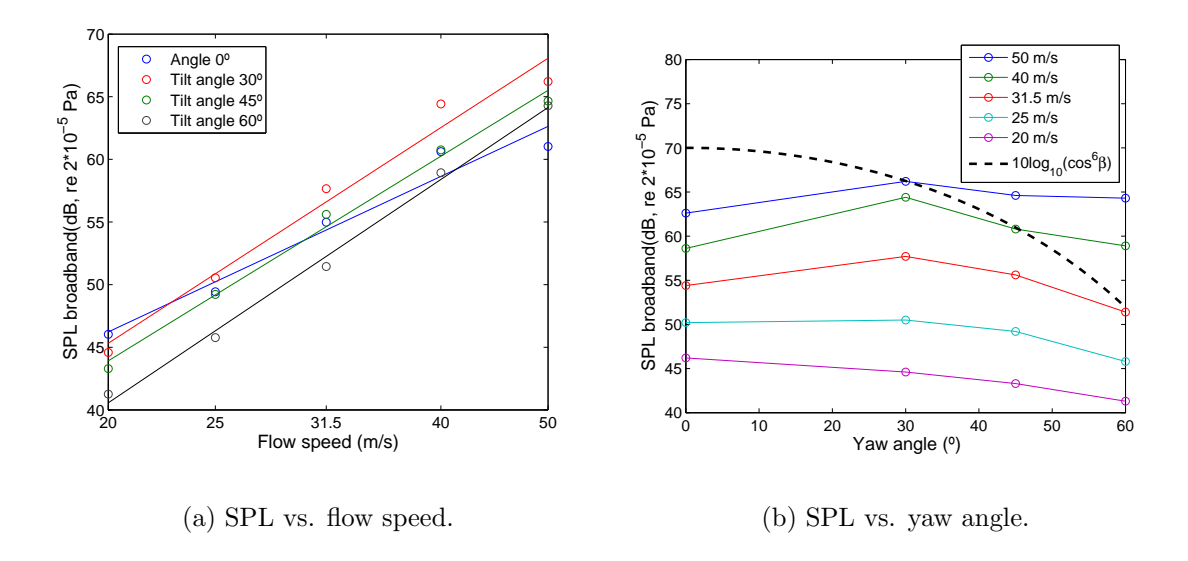


Figure 41: Variation of the broadband SPL with the flow speed and the yaw angle for the elliptical cylinder with eccentricity 0.75.

variations of the SPL with the flow speed for all the yaw angles. The variation of the SPL with the yaw angle is also similar for all the flow speeds. The decrease of the SPL with the yaw angle is less abrupt than the factor of $60log_{10}(\cos(\beta))$.

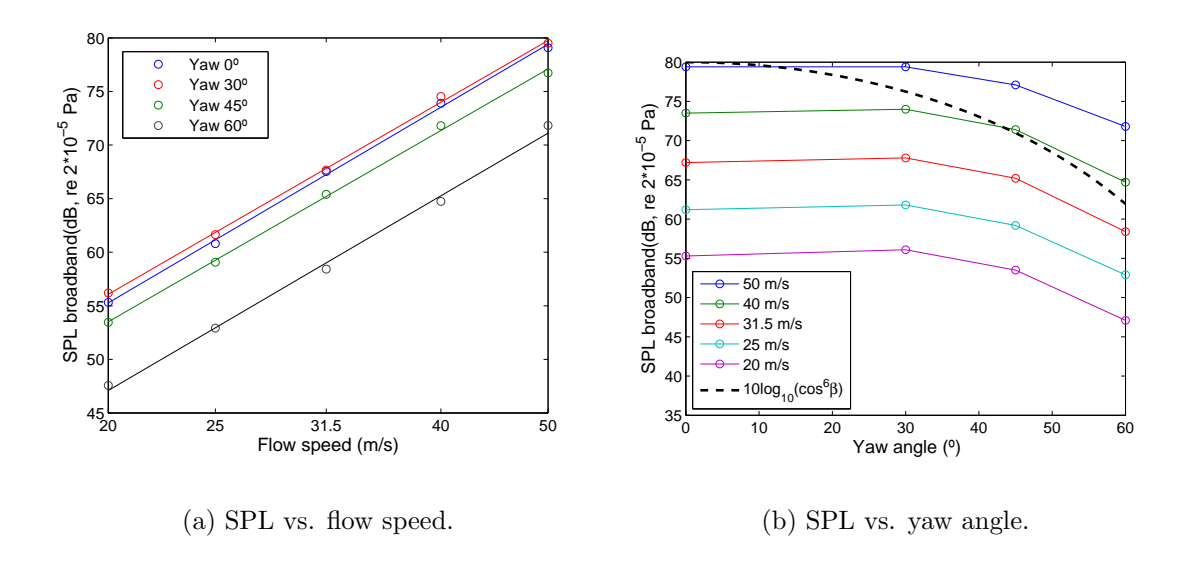


Figure 42: Variation of the broadband SPL with the flow speed and the yaw angle for the rectangular cylinder with aspect ratio of 1.33.

For the rectangular cylinder with aspect ratio of 0.75, the changes in the SPL with the flow speed are quite similar for all the yaw angles, as shown in Figure 43 a). This consistency is also present in the variation of the SPL with the yaw angle for the different flow speeds for angles lower than 60°, as shown in Figure 43 b).

Table 12 gathers the speed exponents of the broadband noise calculated for all the cylinders with different cross-sections and for all the yaw angles evaluated. For the circular cylinder the speed exponent is decreasing with the yaw angle covering a range between 7.0 and 5.6. The reason for

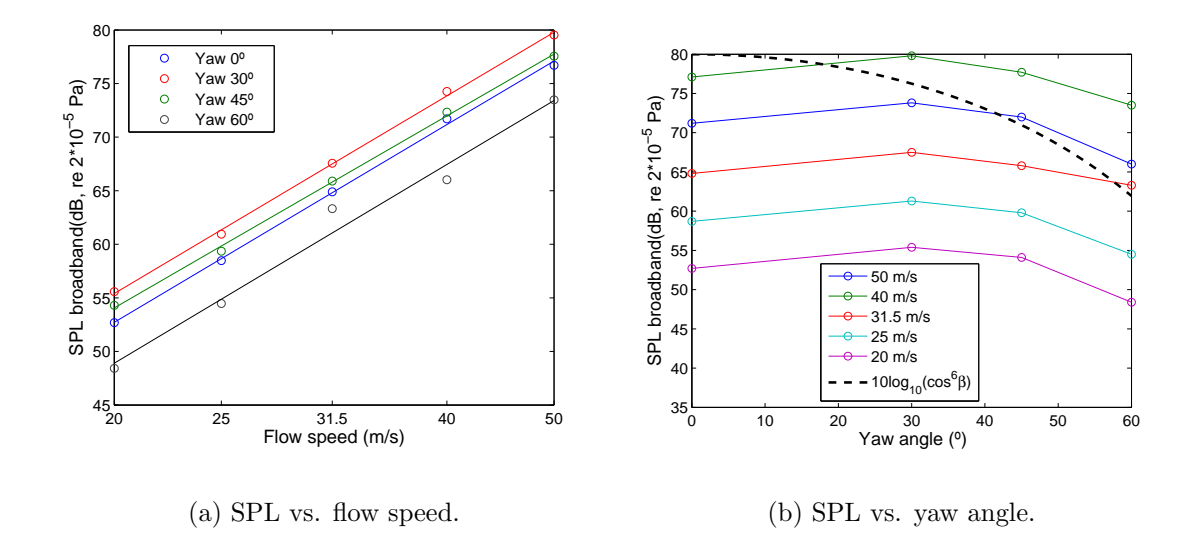


Figure 43: Variation of the broadband SPL with the flow speed and the yaw angle for the rectangular cylinder with aspect ratio of 0.75.

that is not yet understood. This effect is not seen for other cylinder cross-sections. The speed exponent remains quite constant with the yaw angle for the square and rectangular cylinders, with values always around 6.0. For the elliptical cylinders a big variability was found for some of the yaw angles but for most of them the values of the speed exponent fall in the range between 5.5 and 6.5.

Table 12: Speed exponents for different yaw angles for the broadband noise radiated by cylinders with different cross-sections.

Yaw angles β	\mathbf{C}	S	E2	E 1	R1	R1+A90	R2	R2+A90	Sr
0	7.0	6.1	4.1	6.3	6.1	6.1	6.0	6.0	4.8
30	6.4	6.5	5.7	6.2	5.9	6.1	*	*	*
45	6.2	5.9	5.4	5.6	5.9	5.9	*	*	*
60	6.0	6.1	5.9	6.0	6.0	6.2	*	*	*
75	5.6	*	*	*	*	*	*	*	*

In the case of the peak vortex shedding noise the speed exponent was calculated for the frequency where the peak of the noise spectrum was located. For the broadband noise case, the speed exponent is calculated from the overall noise after adding up the noise in each of the frequency bands inside the broadband noise frequency range. In order to understand if the results shown in Table 12 are representative of the variation of the noise with the flow speed in the whole broadband noise frequency range it is then important to assess the variability of the speed exponent with the Strouhal number. This is shown in Figure 44 for the circular and square cylinders yawed by different angles. The speed exponent for each frequency band was found as that which provided the minimum standard deviation after collapsing the noise levels at the different flow speeds. In the case of the circular cylinder, the difference between the speed exponents obtained along the frequency range and the unique value obtained from the overall broadband noise (shown in Table 12) is up to 15%. There is a noticeable decrease of the speed exponent for all the yaw angles for the Strouhal number of 2. The difference is slightly higher for the square cylinder (up to 20%),

with the highest speed exponent occurring for Strouhal numbers between 0.4 and 0.8 (except for the yaw angle of 60°), and decreasing with the Strouhal number for St above 2.5.

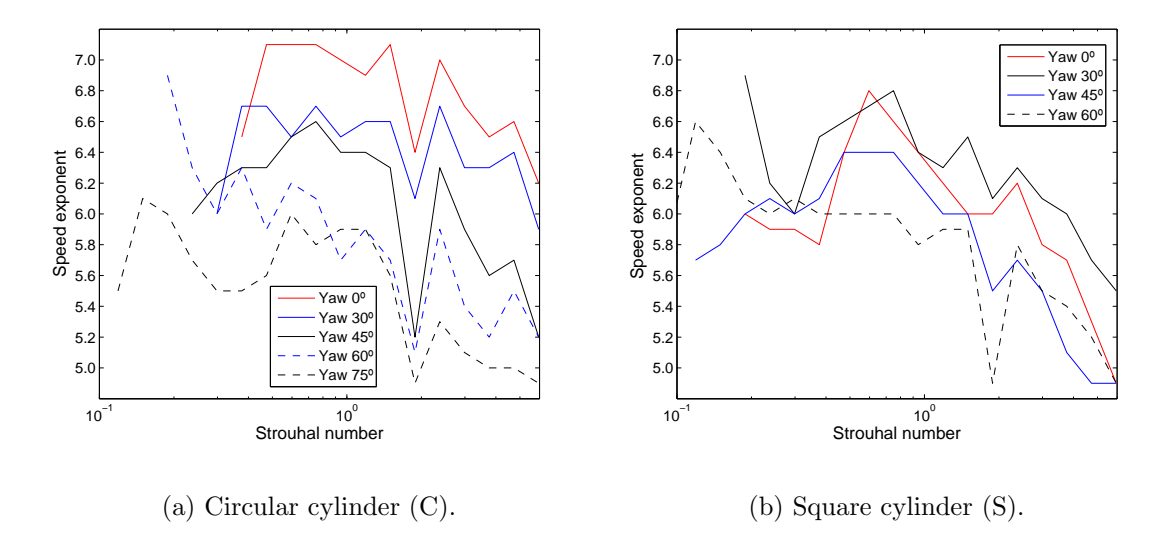


Figure 44: Variability of the speed exponent of broadband noise with the Strouhal number for the circular and square cylinders yawed by different angles.

7.2 Spectral shape

In order to observe any repeated trend in the spectral shape, data obtained for the cylinder cross-sections and for different yaw angles have been collapsed by the flow speed using the speed exponents shown in Table 12 and have been plotted against the Strouhal number. If any common feature is observed in the spectral shape obtained then it can be used for the calibration of semi-empirical prediction models. The Strouhal numbers for the different cylinders are based on the characteristic dimension (D, or b in the case of elliptical cylinders), as shown in Figure 1.

The limited frequency range at low frequencies due to the influence of the background noise makes it impossible to obtain the spectral shape for frequencies lower than the vortex shedding frequencies in many cases such as when the yaw angle is large or the flow speed is low. In such cases, the vortex shedding frequency is close to the low frequency limit of the noise spectrum. For this reason, all the results shown below just consider a broadband frequency range for frequencies above the vortex shedding frequency. However, in some cases it is possible also to see the trend of the broadband noise for frequencies below the vortex shedding frequency. As an example, Figure 45 shows the 1/3 octave noise spectrum from the circular and square cylinder for a flow speed of 50 m/s. The broadband noise in the low-frequency area is circled and it decreases with the decrease of the frequency.

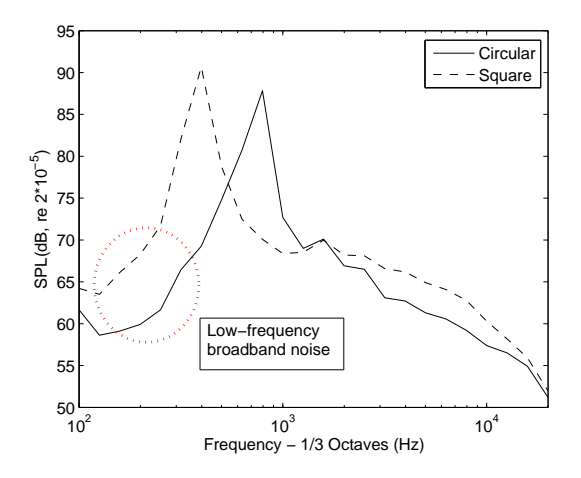


Figure 45: 1/3 octave band noise spectrum for the right circular and square cylinders and for a flow speed of 50 m/s. The broadband noise in the low-frequency range is circled.

In the results shown below presenting the broadband spectra for the different cylinder cross-sections and yaw angles a clearly distinguishable peak was found for a flow speed of 20 m/s. The narrow band noise spectra are shown in Figure 46. There are two very narrow peaks whose frequency is the same for all the yaw angles. The fact that the frequency is independent of the yaw angle lead to conclude that these two peaks are not related to the vortex shedding from the cylinder. These peaks also appear for other cylinder cross-sections for a flow speed of 20 m/s.

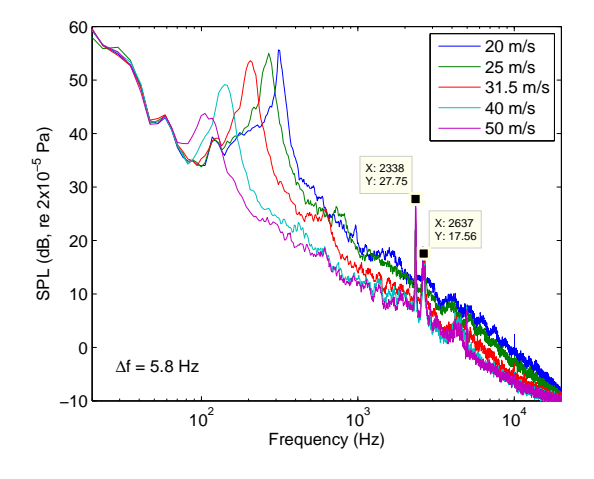


Figure 46: Narrow band spectra for the circular cylinder yawed by different angles for a flow speed of 20 m/s. The frequency of the two narrow distinct peaks is detailed using cursors.

Figure 47 shows the collapsed spectra for a circular cylinder yawed by different angles. The spectral shape seems to be independent of the flow speed but, for large yaw angles and for high Strouhal numbers, the decreasing slopes are slightly different for the different flow speeds.

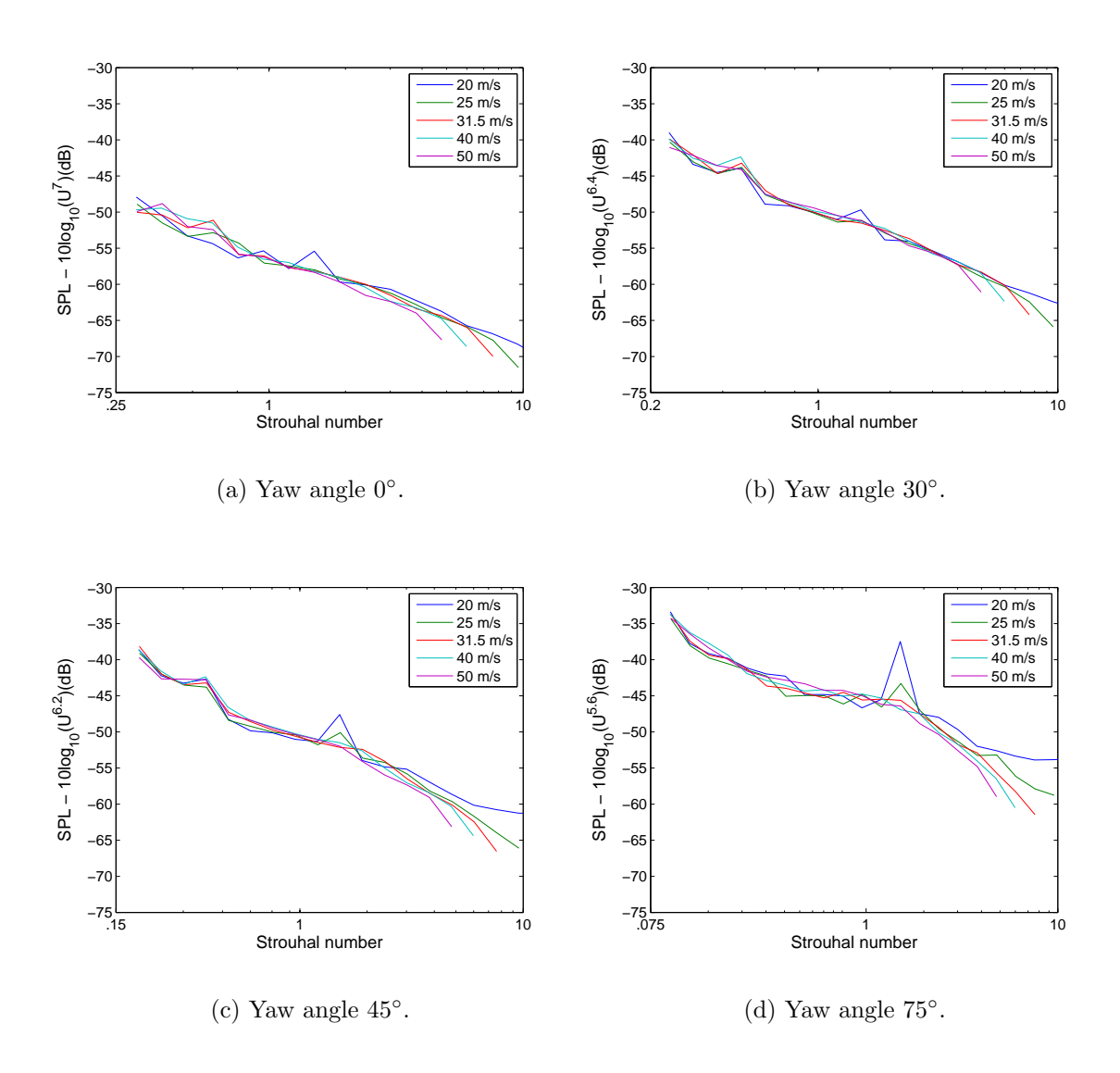


Figure 47: The SPL radiated by a circular cylinder collapsed using the speed exponents shown in Table 12 and plotted against the Strouhal number for different yaw angles β .

For the square cylinder, the spectral shape is quite homogeneous, independent of the flow speed, as shown in Figure 48.

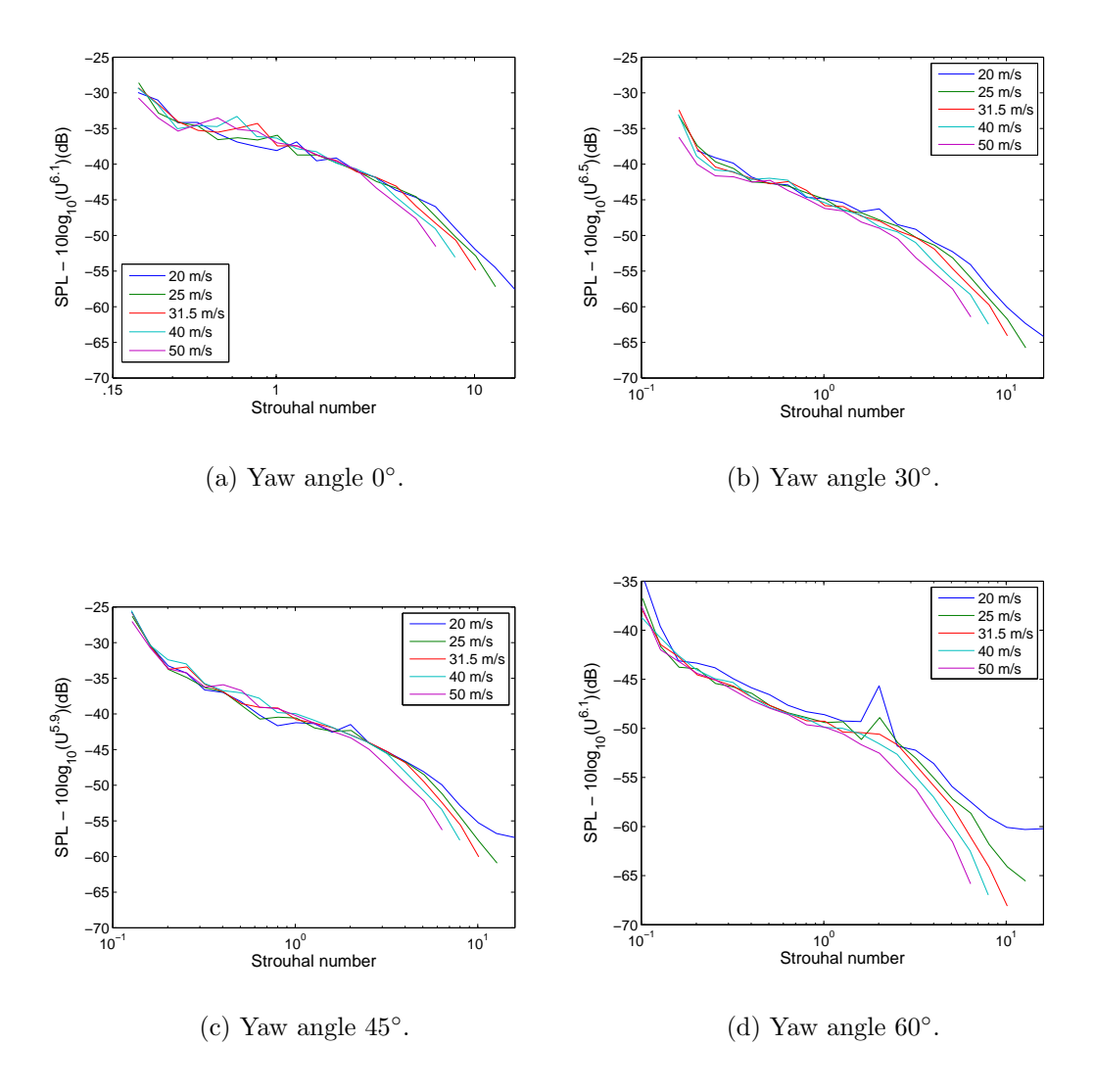


Figure 48: The SPL radiated by a square cylinder collapsed using the speed exponents shown in Table 12 and plotted against the Strouhal number for different yaw angles β .

Similar results to those obtained for the square cylinder have been obtained for the rectangular cylinder with aspect ratio of 1.33. Figure 49 shows a good agreement between the collapsed spectra obtained for the different yaw angles.

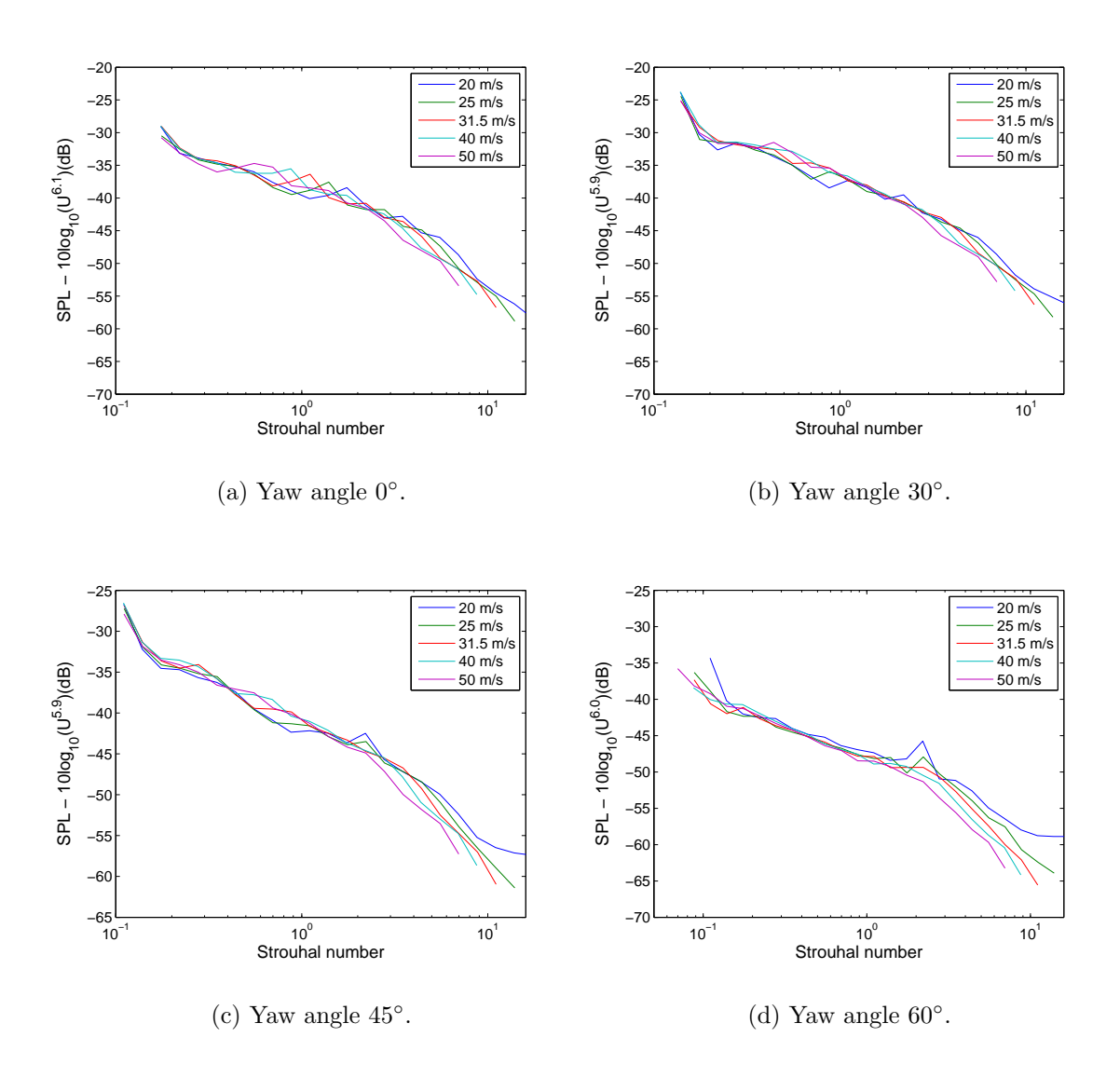


Figure 49: The SPL radiated by a rectangular cylinder with with aspect ratio of 1.33 is collapsed using the speed exponents shown in Table 12 and plotted against the Strouhal number for different yaw angles β .

The trends followed by the average broadband noise spectra from the elliptical cylinder with eccentricity of 0.63 are very similar for yaw angles of 0°, 30° and 45°, as shown in Figure 50. For a yaw angle of 60° it was not possible to find a speed exponent that makes the spectral shapes collapse for the different flow speeds. Figure 40 a) showed that the measurements for this way angle did not fit a straight line trend.

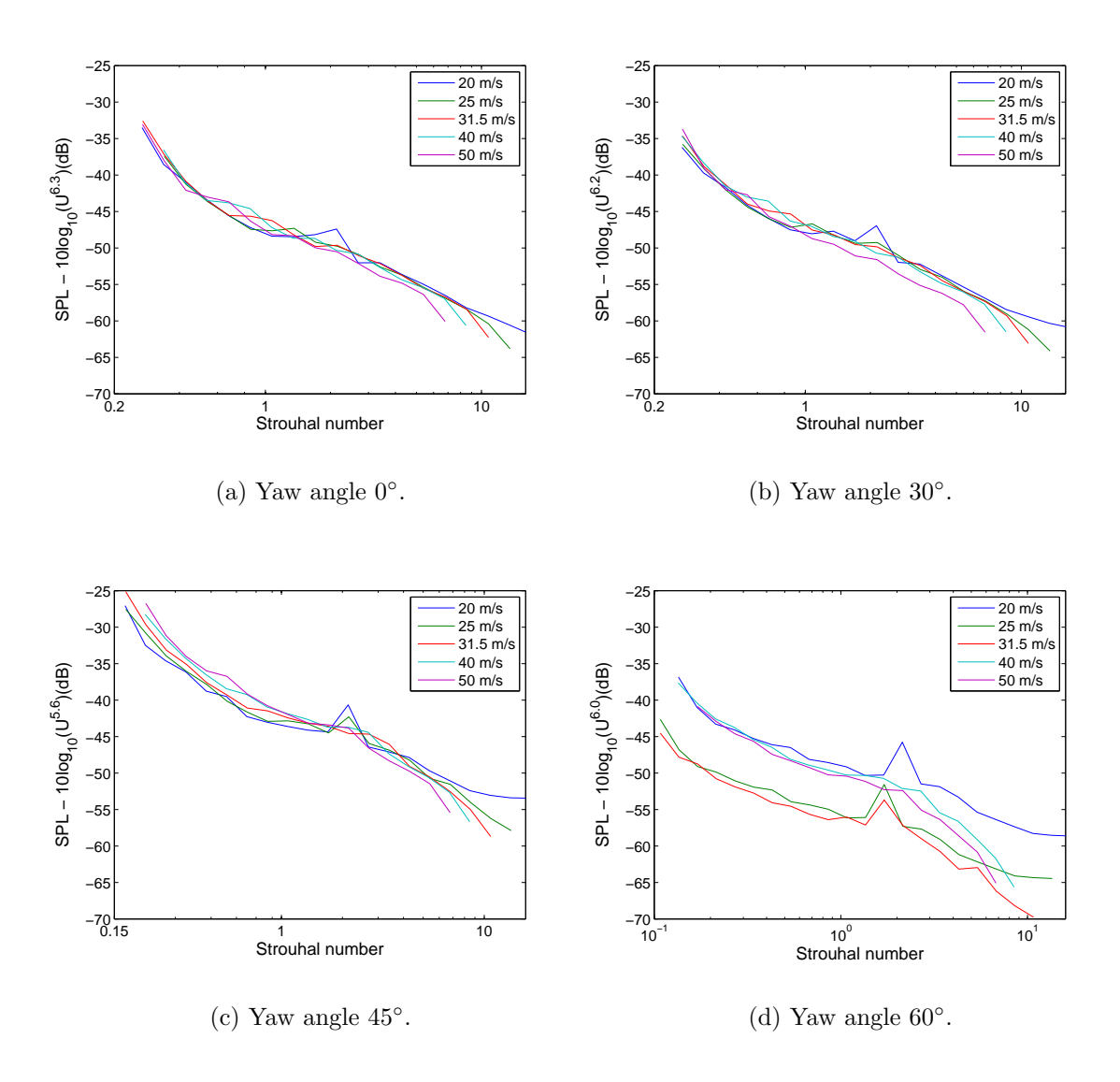


Figure 50: The SPL radiated by an elliptical cylinder with eccentricity of 0.63 is collapsed using the speed exponents shown in Table 12 and plotted against the Strouhal number for different yaw angles β .

For the elliptical cylinder with eccentricity of 0.75, the spectral shape is consistent for different flow speeds for the yaw angles of 0°, 30° and 45°. For a yaw angle of 60°, different slopes are obtained for different flow speeds for Strouhal numbers above 2, as shown in Figure 51.

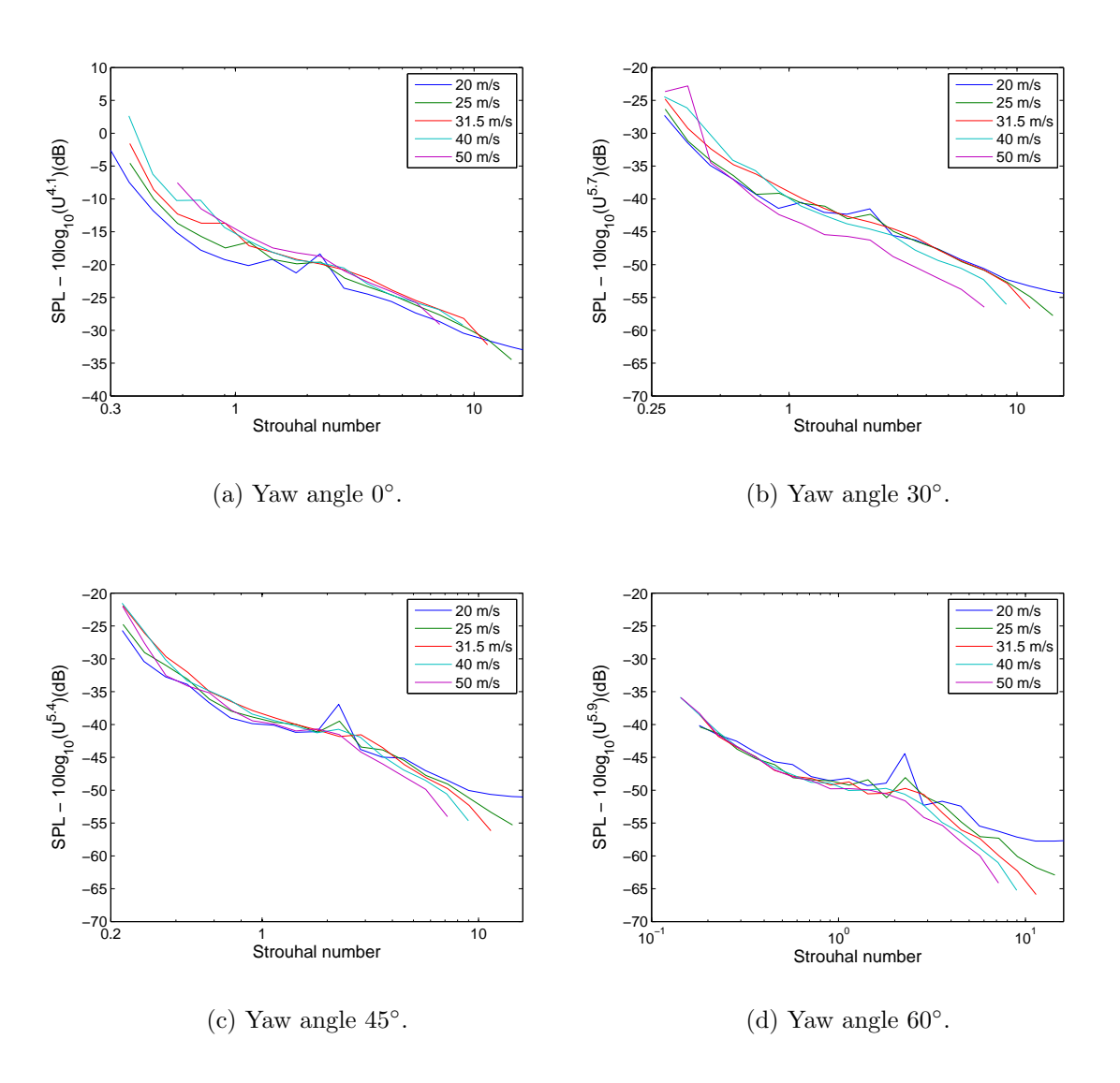


Figure 51: The SPL radiated by an elliptical cylinder with eccentricity of 0.75 is collapsed using the speed exponents shown in Table 12 and plotted against the Strouhal number for different yaw angles β .

In order to assess the influence of the yaw angle on the spectral shape of the broadband noise, the collapsed noise spectra averaged over the different flow speeds for each of the yaw angles are plotted against Strouhal number in Figure 52. The spectral shape is quite consistent with the yaw angle for all the cylinder cross-sections. As a general trend, the spectral shape for the higher yaw angles (60° and 75°) is slightly different than for lower yaw angles, mainly for the highest Strouhal numbers for which the decreasing slope is shallower.

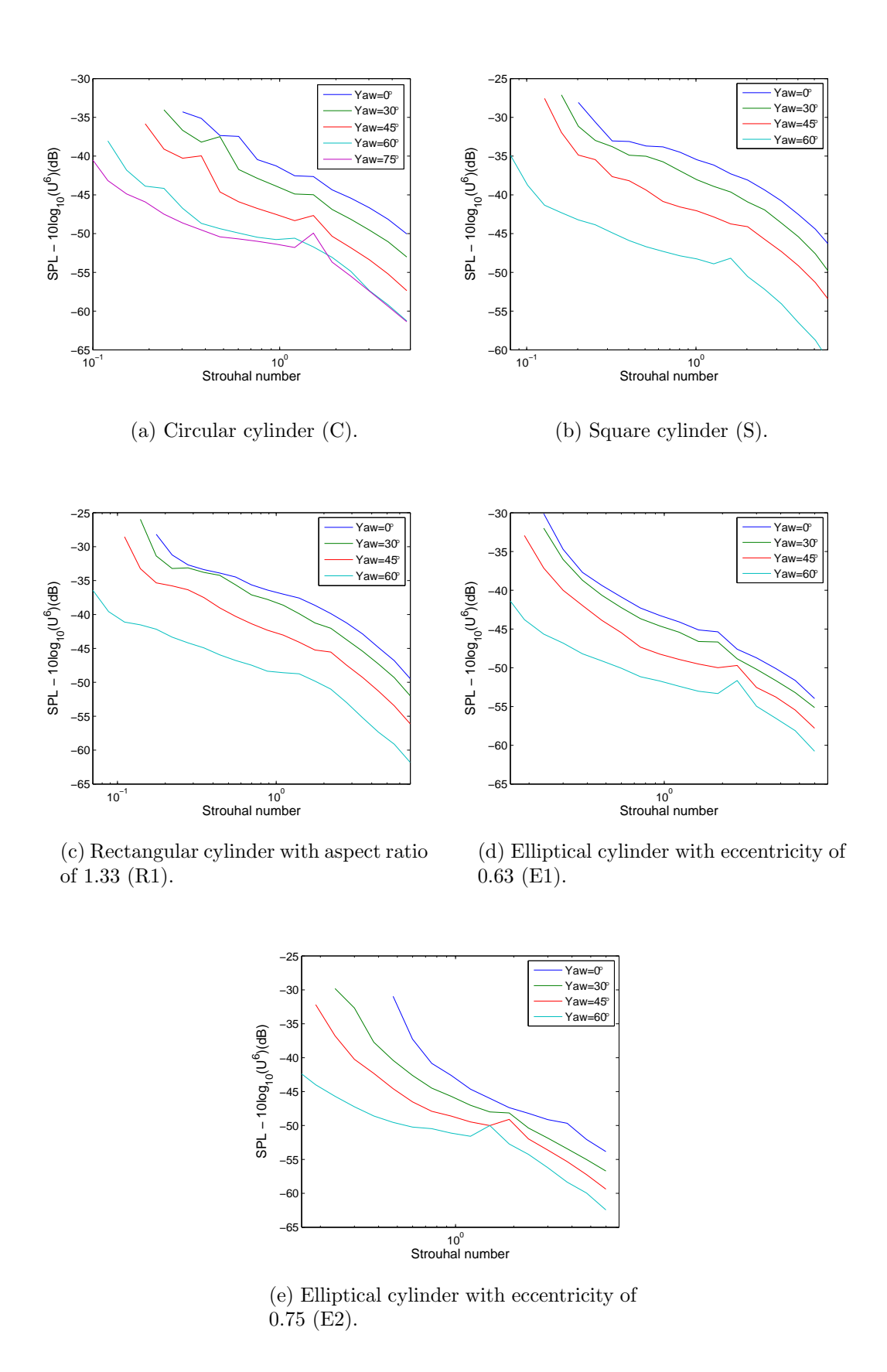


Figure 52: Average noise spectrum collapsed by the flow speed versus Strouhal number for the broadband noise radiated by cylinders with different cross-sections yawed by different angles.

7.3 Directivity of broadband noise

In this section, the directivity patterns of the broadband noise radiated by the circular and square cylinders for yaw angles of 0° and 45° are considered. Unlike the vortex shedding tonal noise the broadband noise is not expected to behave as a pure dipole source.

Figure 53 shows the directivity pattern for the circular and square cylinders for yaw angles 0° and 45°. For all the cases the radiation pattern seems to be far away from that for a theoretical dipole source. The horizontal dotted line included in Figure 53 indicates the radiation pattern expected from an omnidirectional source, with the same radiation in all directions. As a general trend, for radiation angles between 45° and 135° the differences between the omnidirectional radiation pattern and the results are less than 3 dB. For radiation angles higher than 135° the differences are between 3 and 5 dB. The measured directivity pattern seems to be independent of the yaw angle and the cylinder cross-section.

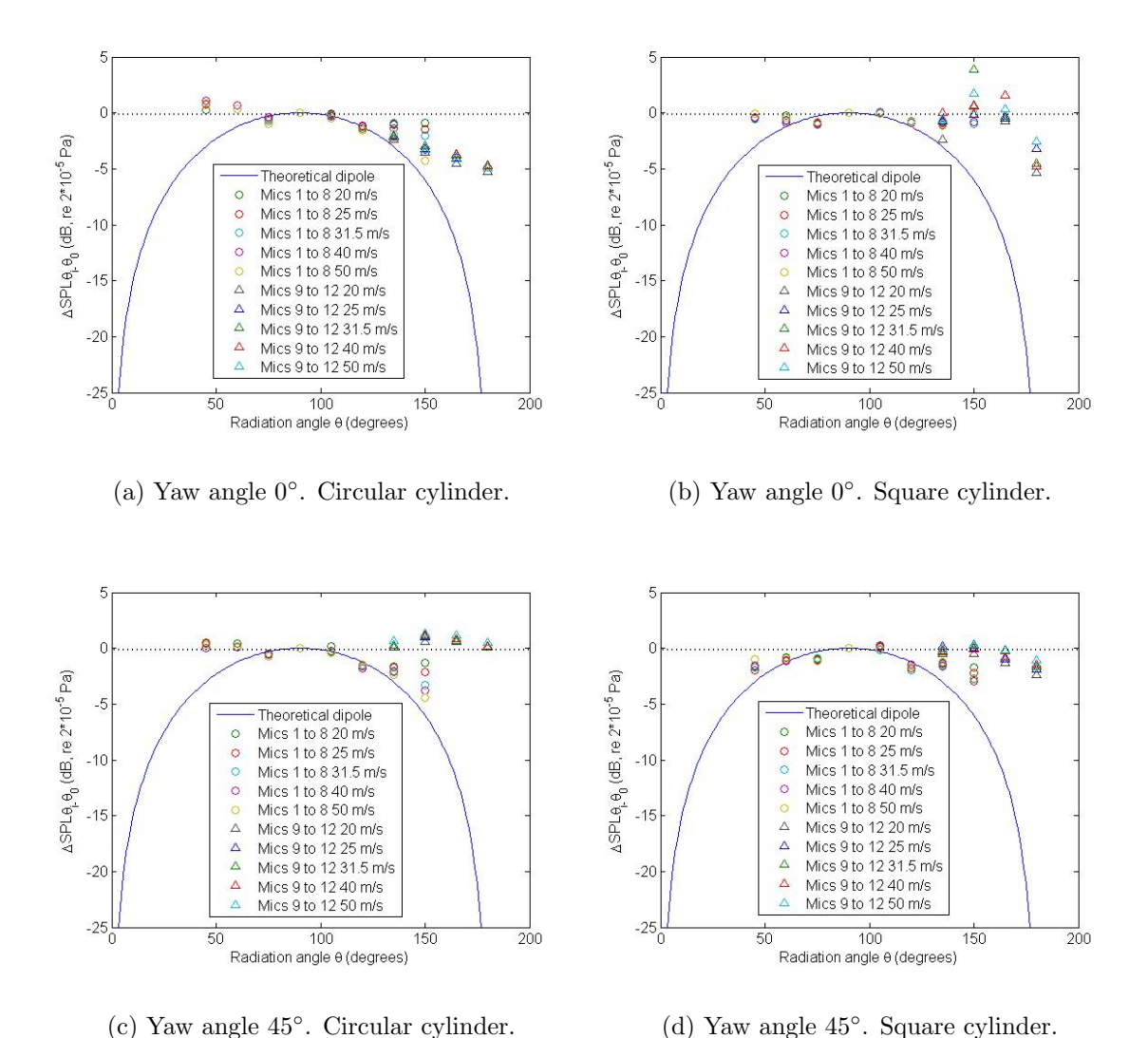


Figure 53: Broadband noise directivity for the circular and square cylinders.

8 Summary of results

The following list summarizes the results obtained for the noise at the vortex shedding frequency. The analysis of the vortex shedding frequency was made by using the narrow band noise spectrum while the analysis of the noise amplitude was made using the maximum value of the 1/3 octave noise spectrum.

- The normalised Strouhal numbers obtained for the square and rectangular cylinders were found to be nearly independent of the flow speed for all the yaw angles, with a small variability of the results. For the circular cylinder, the normalised Strouhal number undergoes a slight increase between the flow speeds of 20 and 31.5 m/s, remaining constant for higher flow speeds. This trend was seen for all the yaw angles except for 75°, for which the Strouhal numbers increased significantly, with values between 0.25 and 0.3, higher than the value of 0.2 expected for an infinite circular cylinder in an air flow in the subcritical region. Finally, for the elliptical cylinders the results show less consistency, with a large variability in the Strouhal number with the flow speed.
- The general trend for all the cases evaluated is a decrease of the Strouhal number with increasing yaw angle. In the case of the circular cylinder the results agrees well with the factor of $\cos(\beta)$ for yaw angles up to 45°, but the measured St is lower than the theoretical result for the yaw angles of 60° and 75°. For the square, rectangular (aspect ratios of 1.33 and 0.75) and elliptical cylinders (eccentricity of 0.63 and 0.75) the variation of St with the yaw angle is in good agreement with the factor of $\cos(\beta)$. The variability is small for the different flow speeds.
- The noise radiated increased as the flow speed increased. If it is assumed that the noise radiated by the fluctuating forces generated on the cylinder due to the vortex shedding process can be defined as a dipole source, then the noise amplitude should increase by a factor (speed exponent) of 6. From the slope of the straight lines obtained when the noise amplitude was plotted against the flow speed, obtained after applying linear curve fitting, the speed exponent for all the cylinder cross-sections was obtained for each of the yaw angles. All the speed exponents obtained are summarized in Table 13.

Table 13: Speed exponents for different yaw angles for the peak noise radiated by cylinders with different cross-sections.

Yaw angles β	\mathbf{C}	S	E2	E 1	R1	R1+A90	R2	R2+A90
0	6.5	5.6	6.0	6.5	5.6	5.5	5.1	5.2
30	6.0	5.9	4.5	8.2	5.5	5.5	*	*
45	6.1	6.0	4.6	9.4	5.7	5.9	*	*
60	6.2	5.5	4.9	5.9	6.9	6.2	*	*
75	6.1	*	*	*	*	*	*	*

• A good agreement was found between the decrease of the amplitude with the yaw angle measured and obtained by using a factor of $\cos^4(\beta)$ for the circular and square cylinders, whereas the decrease of the noise with the yaw angle obtained with the factor $\cos^6(\beta)$ too great.

- As a general conclusion, the trend found in the directivity measured for all the right cylinders and flow speeds and for the yawed circular and square cylinders matches well with the directivity expected for a theoretical dipole source. The variability in the results with the flow speed depends on the case but it is not significant unless the background noise is relevant such as for high yaw angles.
- It was found for a square cylinder that the vortex shedding stopped being triggered at an angle of attack between 10° and 15° . When the cylinder was rotated by 10° no significant changes in St were found and a slight decrease of the SPL was measured. For angles of attack of 15° , 30° and 45° the noise was mainly broadband and no peak was found in the noise spectrum. However, when the cylinder edges were rounded with a radius of D/12, the effect of the angle of attack on St and the noise level was different to that found for the square cylinder with sharp edges. The Strouhal number increased from 0.12 to 0.18 when the rounded square cylinder was rotated by 10° , decreasing to a value of 0.16 for an angle of attack of 30° . The vortex shedding noise level followed the opposite trend. A decrease of 2 dB was obtained for an attack angle of 10° while an increase of 4 dB was obtained for an angle of 30° .

The results obtained for the broadband noise produced by the interaction between the flow and the cylinder undergoing a vortex shedding process are listed below:

- The variation of the SPL with the yaw angle for the different cylinder cross-sections was compared with that obtained by using a theoretical factor of $\cos^6(\beta)$ and, as a general trend, the results did not agree well for higher yaw angles because the decreasing slope from the measurements was shallower. This slope seems to be different for the different cylinder cross-sections. Further analysis must be done on calculating the exponent of the theoretical factor that better fits the results from the measurements.
- For the square and the rectangular cylinders the speed exponents were consistent for different yaw angles and the values were close to the value of 6 expected for a theoretical dipole source. For the elliptical cylinders a higher variability with the yaw angles was obtained with values of the speed exponent between 5.5 and 6.5. In the case of the circular cylinder the speed exponent decreased with the yaw angle from a value of 7.0 for a yaw angle of 0° to a value of 5.6 for a yaw angle of 60°.
- The variation of the speed exponent with the Strouhal number obtained over the frequency range was up to 15% for the circular cylinder yawed by different angles and up to 20% for the square cylinder yawed by different angles.
- The broadband noise spectral shape was found to be very consistent both with the flow speed and yaw angle variations. The trends found for the different cylinders can be used for calibration of the prediction model.
- The average spectral shape was found to be quite consistent for the different yaw angles although for the yaw angles of 60° and 75° the decreasing slope at high frequencies was smaller.
- The directivity of the broadband noise was found to be close to that expected for a monopole source. The differences between the results and the omnidirectional radiation pattern were up to 3 dB for radiation angles between 45° and 135° and between 3 and 5 dB for higher

radiation angles. The directivity pattern measured seems to be independent of the yaw angle and the cylinder cross-section.

The results presented have extended measured data available [1, 2] to include:

- A more extensive study of the effect of the yaw angle on the vortex shedding noise, including higher yaw angles than those available in the literature (60° and 75°) for circular, square, rectangular and elliptical cylinder cross-sections. These angles are in the range of the inclination angles that the main and control struts of a high-train speed pantograph has when operating.
- The noise generated by rectangular and elliptical cylinder was studied for different aspect ratios and eccentricities that those found in the literature, increasing the number of cases available
- The effect of rounding the edges of a square cylinder was studied for a radius of D/12, which is different to the radius used in other cases found in the literature.
- The effect of the angle of attack on the vortex shedding noise was studied for a square cylinder with sharp and rounded edges.
- The directivity of the vortex shedding peak noise was measured for circular, square, rectangular and elliptical cylinders assessing the effect of the yaw angle in the directivity pattern. The symmetry of the results in both the longitudinal and transversal plane was confirmed.
- Several features of the broadband noise radiated by the cylinders were studied for the different cylinder cross-sections: the speed dependence, the effect of the flow speed and yaw angle in the amplitude and shape of the broadband noise spectrum and the directivity pattern.

References

- [1] W.F. King, E.Pfizenmaier, An experimental study of sound generated by flows around cylinders of different cross-section. Journal of Sound and Vibration 328(3), 318-337 (2009).
- [2] F. V. Hutcheson, T. F. Brooks, Noise radiation from single and multiple rod configurations. International Journal of Aeroacoustics 11(3), 291-334 (2012).
- [3] N. Curle. The influence of solid boundaries upon aerodynamic sound. Proceedings of the Royal Society of London. Series A. Mathematical and Physical Sciences 231(1187), 505-514 (1955).
- [4] O.M. Phillips, The intensity of Aeolian tones. Journal of Fluid Mechanics 1(6), 607-624 (1956).
- [5] B. Etkin, G.K. Korbacher, R.T. Keefe. Acoustic radiation from a stationary cylinder in a fluid stream (Aeolian tones). The Journal of the Acoustical Society of America 29(1), 30-36 (1957).
- [6] R.T. Keefe. Investigation of the fluctuating forces acting on a stationary circular cylinder in a subsonic stream and of the associated sound field. The Journal of the Acoustical Society of America, 34(11), 1711-1714 (1962).
- [7] H. Fujita, H. Furutani, H. Suzuki. Experimental investigations and prediction of aerodynamic sound generated from square cylinders. Proceedings of the 4th AIAA/CEAS Aeroacoustics Conference, Tolousse, France, 1998, pp. 2369.
- [8] M.M. Zdravkovich, Flow Around Circular Cylinders, vol. 1. Fundamentals (two volumes). Oxford University Press, Oxford, 1997.
- [9] W. K. Blake, Mechanics of Flow-induced Sound and Vibration, vol. 1. General Concepts and Elementary Sources (two volumes). Academic Press, Orlando, Florida, 1986.
- [10] T.P. Chong, P.F. Joshep, P. Davies, Design and performance of an open jet wind tunnel for aero-acoustic measurement. Applied Acoustics 70(4) (2009) 605-614.
- [11] R.K. Amiet, Refraction of sound by a shear layer. Journal of Sound and Vibration 58(4), 467-482 (1978).
- [12] J.D. Hogan, J.W. Hall, Experimental study of pressure fluctuations from yawed circular cylinders. AIAA Journal 49(11), 2349-2356 (2011).
- [13] G. Schewe, On the force fluctuations acting on a circular cylinder in crossflow from subcritical up to transcritical Reynolds numbers. Journal of Fluid Mechanics 133(1) (1983) 265-285.
- [14] R. King, A review of vortex shedding research and its application. Ocean Engineering 4(3), 141-171 (1977).
- [15] P. Leehey, C. E. Hanson. Aeolian tones associated with resonant vibration. Journal of Sound and Vibration 13 (4), 465-483 (1970).
- [16] H. Fujita. Characteristics of the Aeolian tone radiated from two-dimensional cylinders. Proceedings of the 18th International Congress on Acoustics, Kyoto, Japan, 2004.
- [17] E. Latorre Iglesias, D.J. Thompson, M.G. Smith. Component-based model for aerodynamic noise of high-speed trains. Proc. Int. Workshop Railway Noise, Uddevalla, Sweden, 2013.